A Robust Framework to Design Optimal Sensor Locations for TOA or RSS Source Localization Techniques

Augusto Aubry, *Senior Member, IEEE*, Prabhu Babu, Antonio De Maio, *Fellow, IEEE*, Ghania Fatima, *Graduate Student Member, IEEE*, and Nitesh Sahu

***Abstract*—We focus on the problem of finding optimal sensor locations for source localization techniques based on either time of arrival (TOA) or received signal strength (RSS) measurements. Without any specific assumption on the actual source position, we propose a design framework that directly establishes the optimal sensor locations by minimizing suitable Cramer-Rao bound (CRB)-related cost functions. Specifically, we just consider a region where the source is likely to be present and focus on two cost functions: the former relies on the trace/determinant of CRB averaged over a grid of points resulting from the sampling of the surveillance area (shortly average CRB), whereas, the latter leverages the maximum trace/determinant of CRB over the mentioned grid (shortly worst-case CRB). Moreover, each sensor position is constrained to lie within a pre-specified set (deployment constraint set). Hence, we propose an optimization framework based on block majorization-minimization to deal with both the design paradigms. The iterative steps of the technique monotonically decrease the corresponding figure of merit and eventually converge to a stationary point of the design problem. The proposed methodology can also handle the case of nonuniform noise variances. Finally, through various numerical simulations, we show the effectiveness of the developed resource allocation policies.**

***Index Terms*—Majorization-minimization, optimal sensor placement, received signal strength, source localization, time of arrival.**

I. Introduction and Literature Review

SOURCE localization techniques play a central role in various applications including environment sensing via wireless sensor networks (WSN) [1], navigation and control using global positioning system (GPS) [2], target localization using multiple radars [3], and multilateration systems [4]. Given some noise-corrupted location-related sensor measurements, the position of the source is estimated based on various approaches such as time-of-arrival (TOA) [5], time-difference-of-arrival (TDOA) [6], received-signal-strength (RSS) [7], angle-of-arrival (AOA) [8], and frequency-difference-of-arrival (FDOA) [9]. On top of the underlying processing techniques, the accuracy of the estimated source position depends on the source-sensors relative geometry [10], [11] being the estimation error statistical characterization a function of the sensor locations. Therefore, the optimal placement of sensing nodes is of paramount importance for the aforementioned localization applications. A customary approach to design the optimal placement is to derive the Cramer-Rao bound (CRB) for the localization model under consideration and then minimize a CRB-related metric with respect to the sensor locations. In the following, a summary of the literature on optimal sensor deployments for source localization is presented. The presentation of the references is organized in sub-paragraphs grouping techniques relying on similar sensor measurements (i.e., AOA, TDOA and TOA, RSS, hybrid sensing).

AOA-based techniques: The optimal sensing directions for the AOA model in the two-dimensional (2D) case were derived in [12] under the assumption that all sensors have the same noise variances. In the three-dimensional (3D) case, [13] studied the problem of determining the optimized configuration of an acoustic sensor network for underwater target positioning by bearings-only measurements considering a distance-dependent Gaussian noise model, using the trace of the CRB-related metric (referred to as $A-$optimal design criterion) as the performance indicator. In [14], [15], optimized sensor placements strategies were developed for 3D AOA-based localization assuming nonuniform measurement noise variances. The optimal sensor placements problem for 2D AOA-based localization assuming non-uniform noise variances was analyzed using frame theory in [16]. In [17], the problem of optimal access points deployment for the AOA localization model in a 2D scenario was studied in the context of a WiFi-based localization. Still for a 2D scenario, [18] addressed optimal sensor placements for multisource AOA localization under a distance-dependent noise model (considering $A-$optimal design criterion), whereas, [19] focused on the optimal placement of sensors for the AOA-based source localization under some constraints on the sensor

Manuscript received 14 November 2022; revised 20 February 2023; accepted 21 March 2023. Date of publication 27 March 2023; date of current version 21 April 2023. The associate editor coordinating the review of this manuscript and approving it for publication was Prof. Pascal Vallet. The work of A. Aubry and A. De Maio was supported in part by the European Union under the Italian National Recovery and Resilience Plan (NRRP) of NextGenerationEU, partnership on "Telecommunications of the Future" (CUP J33C22002880001, PE00000001 - program "RESTART"). *(Corresponding author: Ghania Fatima.)*

Augusto Aubry and Antonio De Maio are with the Department of Electrical Engineering and Information Technology, Università degli Studi di Napoli "Federico II", I-80125 Napoli, Italy (e-mail: augusto.aubry@unina.it; ademaio@unina.it).

Prabhu Babu, Ghania Fatima, and Nitesh Sahu are with the CARE, IIT Delhi, New Delhi 110016, India (e-mail: prabhubabu@care.iitd.ac.in; ghania.fatima@care.iitd.ac.in; nitesh.sahu@care.iitd.ac.in).

This article has supplementary downloadable material available at https://doi.org/10.1109/TSP.2023.3262182, provided by the authors.

Digital Object Identifier 10.1109/TSP.2023.3262182

positions using the determinant of the CRB-related metric as the optimality criterion (referred to as $D-$optimal design criterion). Recently, the optimal sensor placement for a single AOA sensor with a Gaussian prior was studied in [20] for a stationary target, limiting the search to sensor angular position, and the results were extended to sensor trajectory optimization for manoeuvring target tracking.

TDOA and TOA-based techniques: In 3D scenario, necessary and sufficient conditions were derived in [21] for optimum sensor array geometry minimizing the CRB-related metric for TDOA-based source localization. The solutions to the optimal sensor placements problem for TDOA-based localization in 2D case were provided in [22] under an uncertain source location. In [23], the optimal geometric configuration for a sensor array located at the sea surface was studied for multiple targets localization in 3D contexts using acoustic range information while considering a distance-dependent noise model. The authors of [24] derived the optimized placement of receivers for elliptical positioning in 3D sensing contexts minimizing the localization error. In [25], optimal centralized and decentralized sensor–pair geometries for the TDOA model were studied (considering the $A-$optimal design criterion), whereas, [26] came up with the selection of the sensing directions for elliptical TOA-based localization in 2D case (employing the $D-$optimal design method). The authors of [27] discussed the optimal placement of jammers in 2D case minimizing a CRB-related metric for wireless localization systems. In [28], the optimal placement for acoustic sensors to localize an underwater target was addressed in 3D using range measurements employing the $D-$optimal criterion. In [29], the optimal placement of anchor nodes was investigated for ultrasound TDOA positioning in 2D via constrained minimization of the geometrical dilution of precision (GDOP). For the 3D case, [30] derived the optimized sensor placements strategies by optimizing the $A-$optimal criterion for different localization models. In [31], the optimal placement for the TOA-based sensors for the simultaneous localization of two targets in 2D was studied. Under constraints on the sensor positions in a 2D scenario, [32] determined the optimal sensors-target geometry for range-based positioning using the $A-$optimality, $E-$optimality, and $D-$optimality criteria, whereas, [33] addressed the optimal sensors-source geometry for the TDOA-based localization by employing the $D-$optimal framework.

RSS-based techniques: The authors of [34] derived the optimal RSS sensors-target geometries for different numbers of applied sensors in 2D scenario. In [35], the optimized placement of anchor nodes with deployment constraints was addressed for an indoor RSS localization system based on a Wireless Sensor Network (WSN). For the 3D case, [36] investigated the optimal placement of sensors by minimizing a CRB-related metric employing $A-$optimal design. Furthermore, in [37], the authors developed an optimal sensor placement strategy for the received-signal-strength-difference (RSSD) localization model in 2D case under the assumption that the transmitted power of the source is unknown.

Hybrid sensing techniques: In 2D scenario, [38] derived the velocity orientation of mobile sensors for hybrid TDOA-FDOA localization of a stationary emitter, whereas, [39] derived both the sensor deployment and velocity configurations of UAVs with hybrid TDOA-FDOA sensors for stationary as well as movable emitters. The problem of designing optimal sensing directions for a hybrid localization model (RSS, AOA, and TOA) was addressed in [40], [41] in a 2D scenario. The authors of [41] also designed the optimal sensor orientations for hybrid RSS-TOA localization in a 3D scenario. The problem of constrained optimal sensor placement of heterogeneous range/bearing/RSS sensor networks was considered in [42] in a 2D scenario, whereas, a unified approach for designing the optimal sensor placements for the TOA, TDOA, AOA, and RSS based localization was presented in [43] in a 3D scenario. Other technically sound deployment strategies, with reference to different sensing measurements, e.g., doppler-shift localization, can be found in [44], [45], [46], [47].

Most of the aforementioned works design optimal sensor placements assuming that the source lies at the center (or a roughly known, although supposed exact at the resource allocation stage, position) of the planned geometry layout. As a result, the problem boils down to establishing only optimal sensor orientations (the angles between the source and the sensors). This could represent a restrictive assumption, as the position of the source is generally and practically unknown. As a matter of fact, if the optimal placements were derived based on a coarse estimate of the source position, then the resulting source position estimation process may suffer a severe performance loss due to the mismatched conditions design, i.e., large errors in the final location estimate could eventually and reasonably occur.

Keeping this in mind, the present paper is focused on optimal sensor geometry layout by minimizing two different CRB-related metrics irrespective of actual source position (robust design), exploiting either TOA or RSS measurements. Specifically, it is considered a sensing area (or volume) over which the source presence is likely to occur (hereafter this region is referred to as source area/volume, and can be chosen arbitrarily without restrictions on its shape). Hence, for each sensing system, two different cost functions are defined to effectively handle the deployment: the former relies on the average of a specific CRB-related metric over the grid points sampling the source area/volume, whereas, the latter leverages the maximum of the CRB-related metric over the aforementioned grid points. The idea of minimizing the average or the worst-case objective functions is quite natural when the actual source position is unknown and only the region containing it is available. Notably, the key difference between our framework and the bulk of methods from the literature is that the design variables in our case are the actual sensor positions, whereas, for most of the state-of-the-art methods the design variables implicitly boil down to the sensor orientations, because either the source location is assumed known or the sensors are forced to lie on a circle/sphere. Needless to say, when the set of grid points chosen in our design is just a singleton, then our methodology reduces to the approach usually pursued in the open literature. The CRB-related metrics adopted to specify the objective function are either the trace (indicated as $A-$optimal oriented design criterion) or the determinant (denoted as $D-$optimal oriented design criterion) of

TABLE I
COMPARISON BETWEEN RELATED PREVIOUS STUDIES AND THIS PAPER

Paper	Non-uniform noise variance	Optimized all sensor location coordinates	Assumed prior information on source position	Deployment constraints	Numerical approach
[26],[15],[30],[37]	Yes	No	Coarse estimate	No	No
[36], [48]	No	No	Coarse estimate	No	No
[43]	Yes	No	Coarse estimate	No	Yes
[19]	No	Yes	Coarse estimate	Yes	No
[42],[33]	Distance dependent	Yes	Coarse estimate	Yes	No
[32]	Yes	Yes	Coarse estimate	Yes	Yes
This paper	**Yes**	**Yes**	**Inside a sensing area (volume)**	**Yes**	**Yes**

the CRB. Hence, to handle the resulting challenging non-convex optimization problems, innovative solution techniques based on the block-majorization-minimization (referred to as block–MM) framework [49], [50] are devised. The proposed resource allocation strategies are iterative in nature and each step monotonically decreases the design objective of interest as well as provides eventually a stationary solution to the underlying optimization problem (this has been rigorously shown in Appendix A of the supplementary material). Besides, it can easily deal with the cases of uniform and non-uniform variances in the measurement noise. Table I highlights the novelty of this work as compared with some relevant literature.

The key contributions can be summarized as follows:

- Definition and computation of the average and the worst-case CRB-related metrics over the grid points chosen from a prescribed source area, in the context of either TOA or RSS measurements. Formulation of the resource allocation problem exploiting two optimality criteria: $A-$ and $D-$optimal.
- Development of a novel optimization framework leveraging the principle of block–MM to minimize the design objective. This is also complemented with a discussion on the computational complexity and the convergence of the algorithm. As already pointed out, the framework can effectively handle noise measurements with non-uniform variances and quite general deployment constraints on the sensor locations.
- Analysis of interesting case studies showing that the proposed technique can lead to some performance gains with respect to some possible counterparts already available in the open literature.

The rest of the paper is organized as follows: Section II presents the source localization measured data models and the formulation of the sensors deployment problems. Section III introduces the proposed solution techniques (and corresponding algorithms) yielding the optimized sensor placements for the two different sensing networks and the diverse adopted figure of merits. In Section IV, numerical simulations are illustrated, whereas in Section V, concluding remarks and possible future research avenues are discussed.

Notations: Throughout the paper, the following notations have been adopted. $\mathbb{R}^n$ and $\mathbb{R}^{m\times n}$ represent the n-dimensional vector space and $m \times n$ matrix space in the real field, respectively. Scalars, vectors, and matrices have been denoted by standard lowercase letter a, lower case boldface letter $\mathbf{a}$, and upper case boldface letter $\mathbf{A}$, respectively. The symbols $(\cdot)^T$, $(\cdot)^{-1}$, $\mathrm{Tr}(\cdot)$, $\det(\cdot)$, $\ln(\cdot)$, $\|\cdot\|_2$, and $\mathbf{I}_m$ denote the transpose, inverse, trace, determinant, natural logarithm, the Euclidean norm of a vector, and an $m \times m$ identity matrix, respectively. $\mathbf{A} \succeq \mathbf{B}$ indicates that $\mathbf{A} - \mathbf{B}$ is a symmetric positive semidefinite matrix and $\mathrm{diag}(\cdot)$ represents a diagonal matrix made of its vector argument.

II. PROBLEM FORMULATION

In this section, TOA and RSS based localization models are introduced and specific sensor placements problems are formulated to optimally deploy the sensing units.

A. TOA Source Localization Model

Let us consider a multiplatform system composed of m (monostatic and active) sensors each equipped with a transceiver capable of measuring the TOA from a target/source located at an unknown position $\mathbf{p} \in \mathbb{R}^n$ (where n is equal to either 2 or 3, depending on the sensing scenario, i.e., 2D or 3D). Denoting the position of the ith sensor by $\mathbf{r}_i \in \mathbb{R}^n$, $i = 1, \ldots, m$ (with $m > n$ as per-location identifiability), the TOA, resulting from the round-trip time, measured at the ith sensor can be written as[1]

$$\widetilde{t}_i = \frac{2\,\|\mathbf{p} - \mathbf{r}_i\|_2}{c} + \epsilon_i,\ i = 1, \ldots, m, \tag{1}$$

where c indicates the wave propagation speed and ϵ_i represents the TOA measurement noise at the ith sensor, which is modeled as a zero mean Gaussian random variable with variance $\bar{\sigma}_i^2$. The resulting distance measurement is

$$\widetilde{d}_i = \|\mathbf{p} - \mathbf{r}_i\|_2 + \varepsilon_i,\ i = 1, \ldots, m, \tag{2}$$

where $\widetilde{d}_i \triangleq \frac{c\widetilde{t}_i}{2}$ corresponds to the noisy distance measurement and $\varepsilon_i = c\epsilon_i/2 \sim \mathcal{N}(0, \sigma_i^2)$, with $\sigma_i^2 = \frac{c^2\bar{\sigma}_i^2}{4}$. Stacking together the noisy distance measurements from the m sensors, the available location-based observations can be cast in the vectorial form

$$\widetilde{\mathbf{d}} = \mathbf{g}_{\mathrm{TOA}}(\mathbf{p}) + \boldsymbol{\xi}_{\mathrm{TOA}} \tag{3}$$

where $\widetilde{\mathbf{d}} = [\widetilde{d}_1, \ldots, \widetilde{d}_m]^T \in \mathbb{R}^m$, $\mathbf{g}_{\mathrm{TOA}}(\mathbf{p}) = [\|\mathbf{p} - \mathbf{r}_1\|_2, \ldots, \|\mathbf{p} - \mathbf{r}_m\|_2]^T \in \mathbb{R}^m$ and $\boldsymbol{\xi}_{\mathrm{TOA}} = [\varepsilon_1, \ldots, \varepsilon_m]^T \in \mathbb{R}^m$ with

[1] A similar signal model and subsequent design hold true for GNSS.

$\boldsymbol{\xi}_{\text{TOA}} \sim \mathcal{N}(\mathbf{0}, \mathbf{R}_{\text{TOA}})$, where $\mathbf{R}_{\text{TOA}} = \text{diag}(\sigma_1^2, \ldots, \sigma_m^2)$ denotes the measurement noise covariance matrix. Therefore, the joint density function of the observation vector $\widetilde{\mathbf{d}}$ is given by

$$p\left(\widetilde{\mathbf{d}};\mathbf{p}\right) = \frac{1}{(2\pi)^{\frac{m}{2}}\sqrt{\det\left(\mathbf{R}_{\text{TOA}}\right)}} \exp\left(-\frac{1}{2}\left(\widetilde{\mathbf{d}}-\mathbf{g}_{\text{TOA}}(\mathbf{p})\right)^T\mathbf{R}_{\text{TOA}}^{-1}\left(\widetilde{\mathbf{d}}-\mathbf{g}_{\text{TOA}}(\mathbf{p})\right)\right). \tag{4}$$

Hence, the Fisher Information Matrix (FIM) associated with the target location $\mathbf{p}$, i.e.,

$$\mathbf{F}_{\text{TOA}}(\mathbf{p}) = \mathbb{E}\left(\left(\frac{\partial \ln p\left(\widetilde{\mathbf{d}};\mathbf{p}\right)}{\partial \mathbf{p}}\right)\left(\frac{\partial \ln p\left(\widetilde{\mathbf{d}};\mathbf{p}\right)}{\partial \mathbf{p}}\right)^T\right) \in \mathbb{R}^{n\times n}, \tag{5}$$

can be computed in closed form via Slepian-Bangs formula [51]

$$\mathbf{F}_{\text{TOA}}\left(\mathbf{p}\right) = \mathbf{H}^T\mathbf{R}_{\text{TOA}}^{-1}\mathbf{H} \tag{6}$$

where

$$\mathbf{H} \triangleq [\mathbf{h}_1, \quad \cdots, \quad \mathbf{h}_m]^T \triangleq \left[\frac{(\mathbf{p}-\mathbf{r}_1)}{\|\mathbf{p}-\mathbf{r}_1\|_2}, \quad \cdots, \quad \frac{(\mathbf{p}-\mathbf{r}_m)}{\|\mathbf{p}-\mathbf{r}_m\|_2}\right]^T. \tag{7}$$

As a consequence, the CRB matrix, which yields a lower bound to the covariance matrix of any unbiased estimator of the target position, is given by

$$\mathbf{C}_{\text{TOA}}\left(\mathbf{p}, \mathbf{r}_1, \ldots, \mathbf{r}_m\right) = \mathbf{F}_{\text{TOA}}^{-1}\left(\mathbf{p}\right) = \left(\mathbf{H}^T\mathbf{R}_{\text{TOA}}^{-1}\mathbf{H}\right)^{-1}, \tag{8}$$

which depends on the actual target position $\mathbf{p}$ and the location of the m sensors $\mathbf{r}_1, \ldots, \mathbf{r}_m$, via the matrix $\mathbf{H}$. In particular, the functional dependence of (8) on $\mathbf{r}_1, \ldots, \mathbf{r}_m$ highlights that a bespoke deployment of the sensing units represents a valuable degree of freedom which can be capitalized to boost localization performance. In this respect, most of the strategies available in the open literature to optimally control the geometry of the sensors assume that the source position is located at the center of the surveilled area (e.g., the origin). Evidently, such a design assumption may lead to significant performance degradation due to mismatches between nominal and actual situations. Here, to overcome the aforementioned shortcoming, a different approach is pursued, assuming that the source may lie in any position within a specific (but quite arbitrary) region in the sensing scenario. Note that it could be also possible to restrict the uncertainty region exploiting some available a-priori knowledge, for instance, previous measurements and tracking information.

To proceed further, let $\{\mathbf{p}_k\}_{k=1}^K$ be a grid of K locations belonging to the surveillance area $\mathcal{A}$, assumed fine enough to represent, with a given accuracy, the possible target positions of interest. Hence, as figure of merit to perform resource allocation (i.e., sensor placements), some CRB-related objective functions are adopted. Specifically, $A-$optimal and $D-$optimal oriented design criteria are considered. The former [52] aims at minimizing the variance of the location estimate, accounting for the trace of the CRB matrix; the latter [52] focuses on the shrinking of the confidence-ellipsoid volume (associated with the location estimate) by means of CRB matrix determinant as score function. Now, since the CRB matrix depends on the unknown target location, either the average or the worst-case (over the selected grid points chosen within the surveillance area) $A-$optimal and $D-$optimal metrics are employed as figure of merits. Otherwise stated, denoting by

$$f_{1,\text{TOA}}\left(\mathbf{p}, \mathbf{r}_1, \ldots, \mathbf{r}_m\right) = \text{Tr}\left(\mathbf{C}_{\text{TOA}}\left(\mathbf{p}, \mathbf{r}_1, \ldots, \mathbf{r}_m\right)\right) \tag{9}$$

and

$$f_{2,\text{TOA}}\left(\mathbf{p}, \mathbf{r}_1, \ldots, \mathbf{r}_m\right) = \det\left(\mathbf{C}_{\text{TOA}}\left(\mathbf{p}, \mathbf{r}_1, \ldots, \mathbf{r}_m\right)\right), \tag{10}$$

the robust (in the sense that no prior information is required about the exact target position) sensor deployment is pursued adopting as design criteria

$$g_i^{\text{TOA}}\left(\mathbf{r}_1, \ldots, \mathbf{r}_m\right) = \frac{1}{K}\sum_{k=1}^K f_{i,\text{TOA}}\left(\mathbf{p}_k, \mathbf{r}_1, \ldots, \mathbf{r}_m\right), \ i=1,2, \tag{11}$$

to regulate average performance, and

$$h_i^{\text{TOA}}\left(\mathbf{r}_1, \ldots, \mathbf{r}_m\right) = \max_{k\in\{1,\ldots,K\}} f_{i,\text{TOA}}\left(\mathbf{p}_k, \mathbf{r}_1, \ldots, \mathbf{r}_m\right), \ i=1,2, \tag{12}$$

to control the worst-case performance.

To endow practical appeal to the resource allocation strategy, it is valuable and necessary to account for some constraints on the location of the sensing platforms, arising from physical restrictions and/or considerations. In this regard, it is worth observing that the measurement model in (1) demands the sensing units (radars) to be far enough from the target, for practical reasons and in order to avoid undesired phenomena, such as eclipsing effects as well as close-in clutter returns, just to mention a few. Thus, denoting by $\mathcal{R}_i$, $i = 1, \ldots m$, the set of the feasible positions of the ith sensor (also referred to as feasible deployment region), the aforementioned requirement is tantamount to assume $\mathcal{R}_i \cap \mathcal{A} = \varnothing$, $i = 1, \ldots m$, i.e., the sensors are located outside the surveillance region. Besides, in realistic scenarios, licenses are often required to place sensing units in specific areas with resulting location constraints, e.g., on the roofs of building or on the top of a hill; additionally, with reference to a multiplatform sensing system employing Unmanned Aerial Vehicles (UAVs), limitations on the sensor positions (to optimally accomplish possible dynamic tasks) naturally stem from UAVs kinematic constraints. Hence, in the following, the feasible deployment region $\mathcal{R}_i$ of the ith sensor is modeled as a convex set, e.g., a sphere (a circle in 2D case), an ellipsoid, or a box, whose geometric parameters (for instance, the radius and the center for a sphere based constraint) reflect position limitations to impose at the design stage. A notional illustration on the sensing scenario of interest, including the surveillance region as well as the feasible deployment regions, is provided in Fig. 1.

According to the above guidelines and definitions, denoting by

$$\mathbf{H}_k \triangleq [\mathbf{h}_{k,1}, \ldots, \mathbf{h}_{k,m}]^T \triangleq \left[\frac{(\mathbf{p}_k-\mathbf{r}_1)}{\|\mathbf{p}_k-\mathbf{r}_1\|_2}, \ldots, \frac{(\mathbf{p}_k-\mathbf{r}_m)}{\|\mathbf{p}_k-\mathbf{r}_m\|_2}\right]^T, \tag{13}$$

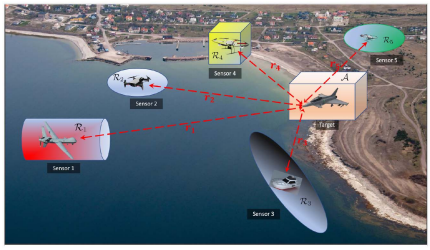

Fig. 1. A pictorial representation of the sensing scenario with $m = 5$ independent transmit/receive units: $\mathcal{A}$ denotes the actual surveillance region while $\mathcal{R}_1 - \mathcal{R}_5$ represent the feasible deployment regions.

the sensor placements problems can be cast as follows

$$\mathcal{P}_1^{TOA}: \underset{\{\mathbf{r}_i \in \mathcal{R}_i\}_{i=1}^m}{\text{minimize}} \ \frac{1}{K}\sum_{k=1}^{K} \text{Tr}\left(\left(\mathbf{H}_k^T \mathbf{R}_{\text{TOA}}^{-1} \mathbf{H}_k\right)^{-1}\right), \quad (14)$$

$$\mathcal{P}_2^{TOA}: \underset{\{\mathbf{r}_i \in \mathcal{R}_i\}_{i=1}^m}{\text{minimize}} \ \frac{1}{K}\sum_{k=1}^{K} \det\left(\left(\mathbf{H}_k^T \mathbf{R}_{\text{TOA}}^{-1} \mathbf{H}_k\right)^{-1}\right), \quad (15)$$

$$\mathcal{P}_3^{TOA}: \underset{\{\mathbf{r}_i \in \mathcal{R}_i\}_{i=1}^m}{\text{minimize}} \ \max_{k\in\{1,\ldots,K\}} \left\{\text{Tr}\left(\left(\mathbf{H}_k^T \mathbf{R}_{\text{TOA}}^{-1} \mathbf{H}_k\right)^{-1}\right)\right\}, \quad (16)$$

$$\mathcal{P}_4^{TOA}: \underset{\{\mathbf{r}_i \in \mathcal{R}_i\}_{i=1}^m}{\text{minimize}} \ \max_{k\in\{1,\ldots,K\}} \left\{\det\left(\left(\mathbf{H}_k^T \mathbf{R}_{\text{TOA}}^{-1} \mathbf{H}_k\right)^{-1}\right)\right\}. \quad (17)$$

B. RSS Source Localization Model

Let us consider a multiplatform system composed of m receiver units (located at $\mathbf{r}_1, \ldots, \mathbf{r}_m$), measuring the RSS from a source located at an unknown position $\mathbf{p} \in \mathbb{R}^n$. Specifically, the RSS measurement at the ith node, i.e., the average power L_i (in dB), can be modeled as

$$L_i = L_0 - 10\,\eta \log_{10}\left(\|\mathbf{p} - \mathbf{r}_i\|_2\right) + \nu_i, \ i = 1, \ldots, m, \quad (18)$$

where L_0 is the received power in dB at a given reference distance, assumed without loss of generality equal to one, η is the (assumed known) path loss exponent, which depends on the propagation channel [53], and ν_i refers to the RSS measurement noise at the ith sensor, which is modeled as a zero mean Gaussian random variable with variance ρ_i^2. Note that, leveraging appropriate calibration procedures [53], [54] the parameters L_0 and η can be assumed known. After stacking together the noisy RSS data from the m sensors, the location-based observations in (18) boil down to

$$\mathbf{y} = \alpha\, \mathbf{g}_{\text{RSS}}(\mathbf{p}) + \boldsymbol{\xi}_{\text{RSS}}, \quad (19)$$

where $\mathbf{y} = [L_1 - L_0, \ldots, L_m - L_0]^T$, $\alpha = -10\eta$, $\mathbf{g}_{\text{RSS}}(\mathbf{p}) = [\log_{10}(\|\mathbf{p} - \mathbf{r}_1\|_2), \ldots, \log_{10}(\|\mathbf{p} - \mathbf{r}_m\|_2)]^T$, and $\boldsymbol{\xi}_{\text{RSS}} = [\nu_1, \ldots, \nu_m]^T \sim \mathcal{N}(\mathbf{0}, \mathbf{R}_{\text{RSS}})$, with $\mathbf{R}_{\text{RSS}} = \text{diag}(\rho_1^2, \ldots, \rho_m^2)$ the covariance matrix of RSS measurements noise. As a consequence, the CRB matrix of any unbiased estimator of the target position, based on RSS measurement model (19), is given by

$$\mathbf{C}_{\text{RSS}}(\mathbf{p}, \mathbf{r}_1, \ldots, \mathbf{r}_m) = \frac{1}{\alpha^2}\left(\mathbf{H}^T \mathbf{D}^T \mathbf{R}_{\text{RSS}}^{-1} \mathbf{D} \mathbf{H}\right)^{-1} \quad (20)$$

where $\mathbf{D} = \text{diag}(\|\mathbf{p} - \mathbf{r}_1\|_2, \ldots, \|\mathbf{p} - \mathbf{r}_m\|_2)^{-1}$ and the matrix $\mathbf{H}$ is defined in (7) and embeds the CRB dependency on the actual target position $\mathbf{p}$ and the sensor locations $\mathbf{r}_1, \ldots, \mathbf{r}_m$. Hence, defining $\mathbf{G} \triangleq \mathbf{D}\mathbf{H}$, i.e.,

$$\mathbf{G} \triangleq [\mathbf{g}_1, \ \cdots, \ \mathbf{g}_m]^T \triangleq \left[\frac{(\mathbf{p}-\mathbf{r}_1)}{\|\mathbf{p}-\mathbf{r}_1\|_2^2}, \ \ldots, \ \frac{(\mathbf{p}-\mathbf{r}_m)}{\|\mathbf{p}-\mathbf{r}_m\|_2^2}\right]^T \quad (21)$$

the CRB matrix in (20) can be cast as

$$\mathbf{C}_{\text{RSS}}(\mathbf{p}, \mathbf{r}_1, \ldots, \mathbf{r}_m) = \frac{1}{\alpha^2}\left(\mathbf{G}^T \mathbf{R}_{\text{RSS}}^{-1} \mathbf{G}\right)^{-1}. \quad (22)$$

Now, following similar lines of reasoning and considerations leading to (14)–(17), and letting

$$\mathbf{G}_k \triangleq [\mathbf{g}_{k,1}, \ldots, \mathbf{g}_{k,m}]^T \triangleq \left[\frac{(\mathbf{p}_k - \mathbf{r}_1)}{\|\mathbf{p}_k - \mathbf{r}_1\|_2^2}, \ldots, \frac{(\mathbf{p}_k - \mathbf{r}_m)}{\|\mathbf{p}_k - \mathbf{r}_m\|_2^2}\right]^T, \quad (23)$$

the sensor placements for RSS based localization can be framed as follows

$$\mathcal{P}_1^{RSS}: \underset{\{\mathbf{r}_i \in \mathcal{R}_i\}_{i=1}^m}{\text{minimize}} \ \frac{1}{K}\sum_{k=1}^{K} \text{Tr}\left(\left(\mathbf{G}_k^T \mathbf{R}_{\text{RSS}}^{-1} \mathbf{G}_k\right)^{-1}\right), \quad (24)$$

$$\mathcal{P}_2^{RSS}: \underset{\{\mathbf{r}_i \in \mathcal{R}_i\}_{i=1}^m}{\text{minimize}} \ \frac{1}{K}\sum_{k=1}^{K} \det\left(\left(\mathbf{G}_k^T \mathbf{R}_{\text{RSS}}^{-1} \mathbf{G}_k\right)^{-1}\right), \quad (25)$$

$$\mathcal{P}_3^{RSS}: \underset{\{\mathbf{r}_i \in \mathcal{R}_i\}_{i=1}^m}{\text{minimize}} \ \max_{k\in\{1,\ldots,K\}} \left\{\text{Tr}\left(\left(\mathbf{G}_k^T \mathbf{R}_{\text{RSS}}^{-1} \mathbf{G}_k\right)^{-1}\right)\right\}, \quad (26)$$

$$\mathcal{P}_4^{RSS}: \underset{\{\mathbf{r}_i \in \mathcal{R}_i\}_{i=1}^m}{\text{minimize}} \ \max_{k\in\{1,\ldots,K\}} \left\{\det\left(\left(\mathbf{G}_k^T \mathbf{R}_{\text{RSS}}^{-1} \mathbf{G}_k\right)^{-1}\right)\right\}. \quad (27)$$

Before concluding this subsection, it is worth pointing out that although problems $\mathcal{P}_i^{TOA}$ and $\mathcal{P}_i^{RSS}$, $i = 1, \ldots, 4$, exhibit similar structural forms, the functional dependency of the cost functions over the optimization variables $\mathbf{r}_1, \ldots, \mathbf{r}_m$ is tightly tailored to TOA and RSS measurement models via the matrices $\mathbf{H}_k$ and $\mathbf{G}_k$, $k = 1, \ldots, K$, respectively. Thus, as thoroughly detailed in the next section, some commonalities are present in the development of the solution methods, even if different bespoke optimization tricks are required to tackle the diverse designs.

III. Design of the Proposed Sensor Placements Methods

In this section, novel solution techniques are devised to handle the non-linear, non-convex, and challenging design problems $\mathcal{P}_i^{TOA}$ and $\mathcal{P}_i^{RSS}$, $i = 1, \ldots, 4$, and to define optimal (with some theoretical guarantees) sensor placements strategies. To this end, the optimization framework (i.e., block MM) proposed in [49], where the Block Coordinate Descent (BCD) paradigm is combined with Majorization-Minimization (MM) technique, is exploited. Specifically, along the BCD iterations, instead of minimizing the appropriate restriction of the original objective function, a surrogate function (which tightly upperbounds the

aforementioned objective) is optimized. In the next subsections, a brief primer on block-MM is provided and our proposed methods to solve Problems $\mathcal{P}_i^{TOA}$ and $\mathcal{P}_i^{RSS}$, $i=1,\ldots,4$, are thoroughly illustrated.

A. Block MM Principle

As already stated, block MM algorithm merges the BCD and the standard MM [49]. Specifically, the design variable is split into blocks and each of them is treated as an independent vector of variables and updated according to a standard MM approach while keeping fixed the remaining variables blocks. To better illustrate the principle of the Block MM, let us consider the following optimization problem

$$\underset{\mathbf{x}\in\mathcal{X}}{\text{minimize}} \quad f(\mathbf{x}) \tag{28}$$

where $\mathbf{x}\in\mathbb{R}^n$ is the optimization variable partitioned into M blocks as $\mathbf{x}=\left(\mathbf{x}_1^T,\ldots,\mathbf{x}_i^T,\ldots,\mathbf{x}_M^T\right)^T$, with $\mathbf{x}_i\in\mathcal{X}_i\ \forall i$ and $\mathcal{X}=\mathcal{X}_1\times\ldots\times\mathcal{X}_M$. At $(t+1)$th iteration, the blocks are updated as follows:

$$\mathbf{x}_i^{t+1}\in\arg\underset{\mathbf{x}_i\in\mathcal{X}_i}{\text{minimize}}\ g_i\left(\mathbf{x}_i\,|\mathbf{x}^t\right) \tag{29}$$

$$\mathbf{x}_j^{t+1}=\mathbf{x}_j^t,\ \forall j\neq i, \tag{30}$$

where $i=\text{mod}(t+1)_M$, and $g_i(\mathbf{x}_i\,|\mathbf{x}^t)$ is the global upper bound for the restriction of $f(\mathbf{x})$ to the ith block and satisfies the following properties:

$$f\left(\mathbf{x}^t\right)=g_i\left(\mathbf{x}_i^t\,|\mathbf{x}^t\right),\ \forall\mathbf{x}^t\in\mathcal{X},\forall\mathbf{x}_i^t\in\mathcal{X}_i, \tag{31}$$

$$f\left(\mathbf{x}_1^t,\ldots,\mathbf{x}_i,\ldots,\mathbf{x}_M^t\right)\leq g_i\left(\mathbf{x}_i\,|\mathbf{x}^t\right),\ \forall\mathbf{x}^t\in\mathcal{X},\forall\mathbf{x}_i\in\mathcal{X}_i \tag{32}$$

where $\mathbf{x}^t$ is the value taken by $\mathbf{x}$ at the tth iteration. This leads to an update of $\mathbf{x}$ as $\mathbf{x}^{t+1}=\left(\left(\mathbf{x}_1^t\right)^T,\ldots,\left(\mathbf{x}_i^{t+1}\right)^T,\ldots,\left(\mathbf{x}_M^t\right)^T\right)^T$.

Before concluding this section, note that in plain Block MM, the blocks are updated cyclically, i.e., i repeatedly increases from 1 to M. Alternately, some advanced block selection rules, *i.e.*, the Maximum Block Improvement (MBI) [50], can also be adopted. The interested reader may refer to [49], [50], [55], for further details on Block-MM, MBI, and MM.

B. Sensor Placements Problem for TOA Based Localization

The focus of this subsection is the design of solution techniques for Problems $\mathcal{P}_i^{TOA}$, $i=1,\ldots,4$, leading to optimal TOA-based sensors geometry. To this end, in the following the optimization variable $[\mathbf{r}_1^T,\mathbf{r}_2^T,\ldots,\mathbf{r}_m^T]^T\in\mathbb{R}^{nm}$ is split into m blocks, each of them collecting the coordinates of the ith sensor.

1) Solution to Problems $\mathcal{P}_1^{TOA}$ and $\mathcal{P}_3^{TOA}$: First, the procedure to solve Problem $\mathcal{P}_1^{TOA}$ is described and then the necessary modifications to handle $\mathcal{P}_3^{TOA}$ are provided. In order to proceed, let $\{\mathbf{r}_h^t\}_{h=1}^m$ be the optimal placement up to the tth iteration, and let $\mathbf{r}_i$ be the block to be updated at the $(t+1)$th iteration; then, ignoring the scaling factor $\frac{1}{K}$, the restriction of the objective function with respect to the ith block is given by

$$\sum_{k=1}^{K}\text{Tr}\left(\left(\widetilde{\mathbf{A}}_{k,i}^t+\sigma_i^{-2}\mathbf{h}_{k,i}\mathbf{h}_{k,i}^T\right)^{-1}\right) \tag{33}$$

where

$$\widetilde{\mathbf{A}}_{k,i}^t\triangleq\sum_{h=1,h\neq i}^{m}\sigma_h^{-2}\mathbf{h}_{k,h}^t\left(\mathbf{h}_{k,h}^t\right)^T \tag{34}$$

is assumed positive definite hereafter. In this respect, it is worth pointing out that $\widetilde{\mathbf{A}}_{k,i}^t$ is rank deficient if and only if all the the nodes involved in $\widetilde{\mathbf{A}}_{k,i}^t$ lie on a zero-measure set, i.e., a line for the 2D case and a plane for the 3D counterpart. As a consequence, being slight perturbations of the sensor positions unavoidable (due to numerical errors) and being finite the cardinality of the grid of points $\mathbf{p}_k$s, $\widetilde{\mathbf{A}}_{k,i}^t$ is practically full rank. Indeed, focusing on the more challenging 3D situation and supposing, without loss of generality $i=1$, given $\mathbf{r}_2^t$, for all k, $\mathbf{h}_{k,2}^t$ and $\mathbf{h}_{k,3}^t$ are not aligned for almost all feasible positions of $\mathbf{r}_3^t\in\mathcal{R}_3$; besides, for almost all $\mathbf{r}_4^t\in\mathcal{R}_4$, $\mathbf{h}_{k,4}^t$ does not belong to the plane identified by $\mathbf{h}_{k,2}^t$ and $\mathbf{h}_{k,3}^t$, for any k. As a further consideration, it is also reasonable to restrict the feasible positions of $n+1$ sensors among the available m nodes, so that $\widetilde{\mathbf{A}}_{k,i}^t$ is full rank, regardless of the actual sensor positions; this is for instance the case where some sensors are located on the ground with a limited variability (capable of ensuring a reliable surveillance of a region wider than $\mathcal{A}$), whereas other dynamic and moving units are employed to augment the system in the accomplishment of ad-hoc tasks.[2]

Using Sherman–Morrison formula [56] and after standard algebra, (33) can be cast as

$$\sum_{k=1}^{K}\left(\alpha_{k,i}^t-\frac{\mathbf{h}_{k,i}^T\mathbf{A}_{k,i}^t\mathbf{h}_{k,i}}{1+\mathbf{h}_{k,i}^T\mathbf{B}_{k,i}^t\mathbf{h}_{k,i}}\right) \tag{35}$$

where $\alpha_{k,i}^t\triangleq\text{Tr}\left(\left(\widetilde{\mathbf{A}}_{k,i}^t\right)^{-1}\right)$, $\mathbf{A}_{k,i}^t\triangleq\sigma_i^{-2}\left(\widetilde{\mathbf{A}}_{k,i}^t\right)^{-2}$, and $\mathbf{B}_{k,i}^t\triangleq\sigma_i^{-2}\left(\widetilde{\mathbf{A}}_{k,i}^t\right)^{-1}$. Hence, the relationship $\mathbf{h}_{k,i}=\frac{(\mathbf{p}_k-\mathbf{r}_i)}{\|\mathbf{p}_k-\mathbf{r}_i\|_2}$ yields to the following closed form expression of the objective function of $\mathcal{P}_1^{TOA}$ restricted to $\mathbf{r}_i$, given by

$$\phi(\mathbf{r}_i)\triangleq\sum_{k=1}^{K}\left(\alpha_{k,i}^t-\frac{(\mathbf{p}_k-\mathbf{r}_i)^T\mathbf{A}_{k,i}^t(\mathbf{p}_k-\mathbf{r}_i)}{(\mathbf{p}_k-\mathbf{r}_i)^T\mathbf{D}_{k,i}^t(\mathbf{p}_k-\mathbf{r}_i)}\right) \tag{36}$$

where $\mathbf{D}_{k,i}^t=\mathbf{I}_n+\mathbf{B}_{k,i}^t$.

In line with the Block-MM paradigm, let us now focus on the construction of a valuable surrogate function to (36). To this

[2]Note that a slight perturbation of the matrices involved in the objective function can be considered too, i.e., $(\widetilde{\mathbf{A}}_{k,i}^t+\sigma_i^{-2}\mathbf{h}_{k,i}\mathbf{h}_{k,i}^T+\epsilon\mathbf{I})^{-1}$, with $\epsilon>0$ a regularizing/smoothing factor. Interestingly, this perturbed matrix can be interpreted as the covariance matrix of the estimation error associated with the linearized version (around $\mathbf{p}_k$) of the measurement equations in (2) assuming the offset/displacement modeled as a zero mean Gaussian random vector with covariance matrix $\frac{1}{\epsilon}\mathbf{I}$.

end, let us observe that (36) can be written as

$$\sum_{k=1}^{K}\left(\alpha_{k,i}^{t}-\psi_{k}\left(\mathbf{r}_{i},z_{k}\right)\right) \tag{37}$$

where $z_k=(\mathbf{p}_k-\mathbf{r}_i)^T\mathbf{D}_{k,i}^t(\mathbf{p}_k-\mathbf{r}_i)$ and $\psi_k(\mathbf{r}_i,z_k)\triangleq\frac{(\mathbf{p}_k-\mathbf{r}_i)^T\mathbf{A}_{k,i}^t(\mathbf{p}_k-\mathbf{r}_i)}{z_k}$. Since $\psi_k(\mathbf{r}_i,z_k)$ is jointly convex in $\mathbf{r}_i$ and z_k [57], the following inequality, based on first order Taylor series (at some given $\mathbf{r}_i^t$ and z_k^t), holds true

$$\begin{aligned}\psi_{k}\left(\mathbf{r}_{i},z_{k}\right)&\geq\psi_{k}\left(\mathbf{r}_{i}^{t},z_{k}^{t}\right)+\frac{-2\left(\mathbf{p}_{k}-\mathbf{r}_{i}^{t}\right)^{T}\mathbf{A}_{k,i}^{t}}{z_{k}^{t}}\left(\mathbf{r}_{i}-\mathbf{r}_{i}^{t}\right)\\&\quad-\frac{\left(\mathbf{p}_{k}-\mathbf{r}_{i}^{t}\right)^{T}\mathbf{A}_{k,i}^{t}\left(\mathbf{p}_{k}-\mathbf{r}_{i}^{t}\right)}{\left(z_{k}^{t}\right)^{2}}\left(z_{k}-z_{k}^{t}\right)\\&=\left(\mathbf{a}_{k,i}^{t}\right)^{T}\mathbf{r}_{i}-b_{k,i}^{t}z_{k}+c_{k,i}^{t}\end{aligned} \tag{38}$$

where $\mathbf{a}_{k,i}^t=\frac{-2\mathbf{A}_{k,i}^t(\mathbf{p}_k-\mathbf{r}_i^t)}{(\mathbf{p}_k-\mathbf{r}_i^t)^T\mathbf{D}_{k,i}^t(\mathbf{p}_k-\mathbf{r}_i^t)}$, $b_{k,i}^t=\frac{(\mathbf{p}_k-\mathbf{r}_i^t)^T\mathbf{A}_{k,i}^t(\mathbf{p}_k-\mathbf{r}_i^t)}{((\mathbf{p}_k-\mathbf{r}_i^t)^T\mathbf{D}_{k,i}^t(\mathbf{p}_k-\mathbf{r}_i^t))^2}$ and $c_{k,i}^t=\psi(\mathbf{r}_i^t,z_k^t)-(\mathbf{a}_{k,i}^t)^T\mathbf{r}_i^t+b_{k,i}^tz_k^t$. Now, denoting by $g_k(r_i)=\psi_k(\mathbf{r}_i,(\mathbf{p}_k-\mathbf{r}_i)^T\mathbf{D}_{k,i}^t(\mathbf{p}_k-\mathbf{r}_i))$ and replacing $z_k=(\mathbf{p}_k-\mathbf{r}_i)^T\mathbf{D}_{k,i}^t(\mathbf{p}_k-\mathbf{r}_i)$ in (38), it follows that

$$g_k(\mathbf{r}_i)\geq-\mathbf{r}_i^T\mathbf{F}_{k,i}^t\mathbf{r}_i+\left(\mathbf{w}_{k,i}^t\right)^T\mathbf{r}_i+s_{k,i}^t \tag{39}$$

where $\mathbf{F}_{k,i}^t=b_{k,i}^t\mathbf{D}_{k,i}^t$, $\mathbf{w}_{k,i}^t=\mathbf{a}_{k,i}^t+2b_{k,i}^t\mathbf{D}_{k,i}^t\mathbf{p}_k$, and $s_{k,i}^t=c_{k,i}^t-b_{k,i}^t\mathbf{p}_k^T\mathbf{D}_{k,i}^t\mathbf{p}_k$. As a consequence, a majorizing function for $\phi(\mathbf{r}_i)$ at $\mathbf{r}_i=\mathbf{r}_i^t$ is

$$\phi\left(\mathbf{r}_{i}\right)\leq\sum_{k=1}^{K}\left(\mathbf{r}_{i}^{T}\mathbf{F}_{k,i}^{t}\mathbf{r}_{i}-\left(\mathbf{w}_{k,i}^{t}\right)^{T}\mathbf{r}_{i}+\beta_{k,i}^{t}\right), \tag{40}$$

where $\beta_{k,i}^t\triangleq\alpha_{k,i}^t-s_{k,i}^t$. Therefore, $\mathbf{r}_i^{t+1}$ is obtained as the optimal solution to the following surrogate problem

$$\underset{\mathbf{r}_i\in\mathcal{R}_i}{\text{minimize}}\quad\sum_{k=1}^{K}\left(\mathbf{r}_{i}^{T}\mathbf{F}_{k,i}^{t}\mathbf{r}_{i}-\left(\mathbf{w}_{k,i}^{t}\right)^{T}\mathbf{r}_{i}+\beta_{k,i}^{t}\right) \tag{41}$$

which can be further cast as

$$\underset{\mathbf{r}_i\in\mathcal{R}_i}{\text{minimize}}\quad\mathbf{r}_{i}^{T}\mathbf{F}_{i}^{t}\mathbf{r}_{i}-\left(\mathbf{w}_{i}^{t}\right)^{T}\mathbf{r}_{i}+\beta_{i}^{t} \tag{42}$$

where $\mathbf{F}_i^t=\sum_{k=1}^K\mathbf{F}_{k,i}^t$, $\mathbf{w}_i^t=\sum_{k=1}^K\mathbf{w}_{k,i}^t$ and $\beta_i^t=\sum_{k=1}^K\beta_{k,i}^t$.

Since $\mathbf{F}_i^t\succ\mathbf{0}$, Problem (42) is convex and its solution can be obtained using convex programming solvers, like CVX [58]. In particular, if each $\mathcal{R}_i$ is representative of a practically reasonable region, i.e., a sphere, an ellipsoid, or a box, (42) can be cast as a Second Order Cone Program (SOCP) [57] and solved again via CVX [58]. Remarkably, under the last assumption on $\mathcal{R}_i$'s, the optimal solution in almost closed-form can be obtained leveraging Karush-Kuhn-Tucker (KKT) conditions. After the update of all the sensor locations in a loop, i.e., the execution of m iterations, the resource allocation process is repeated until convergence and a minimizer of Problem $\mathcal{P}_1^{TOA}$ is possibly obtained. In this respect, as detailed in Section III-D, the developed optimization scheme exhibits desirable properties such as a decreasing behavior of the objective function along the iteration and a guaranteed convergence to a stationary point of the minimization problem under some mild technical conditions [55].

The procedure to solve Problem $\mathcal{P}_3^{TOA}$ is now illustrated. Leveraging the similarity between the objectives in $\mathcal{P}_1^{TOA}$ and $\mathcal{P}_3^{TOA}$ (except for the presence of max operator in $\mathcal{P}_3^{TOA}$), the counterpart to Problem (41) can be readily obtained as follows

$$\underset{\mathbf{r}_i\in\mathcal{R}_i}{\text{minimize}}\quad\max_{k}\left\{\mathbf{r}_{i}^{T}\mathbf{F}_{k,i}^{t}\mathbf{r}_{i}-\left(\mathbf{w}_{k,i}^{t}\right)^{T}\mathbf{r}_{i}+\beta_{k,i}^{t}\right\}. \tag{43}$$

Problem (43) can be efficiently handled resorting to its epigraph form, i.e.,

$$\begin{aligned}&\underset{\mathbf{r}_i\in\mathcal{R}_i,\theta}{\text{minimize}}\quad\theta\\&\text{subject to}\quad\mathbf{r}_{i}^{T}\mathbf{F}_{k,i}^{t}\mathbf{r}_{i}-\left(\mathbf{w}_{k,i}^{t}\right)^{T}\mathbf{r}_{i}+\beta_{k,i}^{t}\leq\theta,\forall k,\end{aligned} \tag{44}$$

where θ is an auxiliary variable. Indeed, (44) is a convex optimization problem and can be solved using appropriate convex programming solvers. Furthermore, provided that $\mathcal{R}_i$, $i=1,\ldots,m$, is described by linear inequalities and/or quadratic constraints, (44) can be cast as a SOCP [57].

2) Solution to Problems $\mathcal{P}_2^{TOA}$ and $\mathcal{P}_4^{TOA}$: Now, solution techniques to Problems $\mathcal{P}_2^{TOA}$ and $\mathcal{P}_4^{TOA}$ are presented. Focusing on $\mathcal{P}_2^{TOA}$ and letting $\mathbf{r}_i$ the block to be updated at the $(t+1)$th iteration, with $i=\text{mod}(t+1)_m$, the restriction of the objective function (with respect to the ith block) is

$$\sum_{k=1}^{K}\det\left(\left(\widetilde{\mathbf{A}}_{k,i}^{t}+\sigma_{i}^{-2}\mathbf{h}_{k,i}\mathbf{h}_{k,i}^{T}\right)^{-1}\right), \tag{45}$$

where the scaling factor $\frac{1}{K}$ is neglected. Now, leveraging Sherman–Morrison formula and after some standard algebra, (33) can be equivalently expressed as

$$\sum_{k=1}^{K}\det\left(\left(\widetilde{\mathbf{A}}_{k,i}^{t}\right)^{-1}-\frac{\sigma_{i}^{-2}\left(\widetilde{\mathbf{A}}_{k,i}^{t}\right)^{-1}\mathbf{h}_{k,i}\mathbf{h}_{k,i}^{T}\left(\widetilde{\mathbf{A}}_{k,i}^{t}\right)^{-1}}{1+\sigma_{i}^{-2}\mathbf{h}_{k,i}^{T}\left(\widetilde{\mathbf{A}}_{k,i}^{t}\right)^{-1}\mathbf{h}_{k,i}}\right) \tag{46}$$

where $\widetilde{\mathbf{A}}_{k,i}\succ\mathbf{0}$ is as in (34). Exploiting the determinant identity $\det(\mathbf{A}+\mathbf{u}\mathbf{v}^T)=(1+\mathbf{v}^T\mathbf{A}^{-1}\mathbf{u})\det(\mathbf{A})$ [59], (45) boils down to

$$\sum_{k=1}^{K}\left(\alpha_{k,i}^{t}-\frac{\mathbf{h}_{k,i}^{T}\mathbf{A}_{k,i}^{t}\mathbf{h}_{k,i}}{1+\mathbf{h}_{k,i}^{T}\mathbf{B}_{k,i}^{t}\mathbf{h}_{k,i}}\right) \tag{47}$$

with $\alpha_{k,i}^t\triangleq\det\left(\left(\widetilde{\mathbf{A}}_{k,i}^t\right)^{-1}\right)$ and $\mathbf{A}_{k,i}^t\triangleq\sigma_i^{-2}\alpha_{k,i}^t(\widetilde{\mathbf{A}}_{k,i}^t)^{-1}$.

Since the objective (47) exhibits the same functional form as (35) (the only difference is in the definition of the parameters $\alpha_{k,i}^t$ and $\mathbf{A}_{k,i}^t$), the framework developed in Section III-B1 can be used to handle $\mathcal{P}_2^{TOA}$. The same conclusion applies to $\mathcal{P}_4^{TOA}$ since its objective function restricted to the ith block can be cast in the same form as the objective of $\mathcal{P}_3^{TOA}$, resorting to the mathematical tricks leading to (47).

C. Sensor Placements Problem for RSS Based Localization

In this subsection, the procedures to solve Problems $\mathcal{P}_1^{RSS}$–$\mathcal{P}_4^{RSS}$ are devised aimed at determining optimal placements for the RSS-based sensors.

1) Solution to Problems $\mathcal{P}_1^{RSS}$ and $\mathcal{P}_3^{RSS}$: Let us start with Problem $\mathcal{P}_1^{RSS}$; owing to the similar structural forms between $\mathcal{P}_1^{RSS}$ and $\mathcal{P}_1^{TOA}$ and exploiting the same steps leading to (35), the restriction of the objective function of $\mathcal{P}_1^{RSS}$ with respect to the ith block can be expressed as

$$\sum_{k=1}^{K}\left(\alpha_{k,i}^t-\frac{\mathbf{g}_{k,i}^T\mathbf{A}_{k,i}^t\mathbf{g}_{k,i}}{1+\mathbf{g}_{k,i}^T\mathbf{B}_{k,i}^t\mathbf{g}_{k,i}}\right) \tag{48}$$

where $\alpha_{k,i}^t\triangleq\mathrm{Tr}\left(\left(\widetilde{\mathbf{A}}_{k,i}^t\right)^{-1}\right)$, $\mathbf{A}_{k,i}^t\triangleq\rho_i^{-2}\left(\widetilde{\mathbf{A}}_{k,i}^t\right)^{-2}$, and $\mathbf{B}_{k,i}^t\triangleq\rho_i^{-2}\left(\widetilde{\mathbf{A}}_{k,i}^t\right)^{-1}$, with $\widetilde{\mathbf{A}}_{k,i}^t\triangleq\sum_{h=1,h\neq i}^{m}\rho_h^{-2}\mathbf{g}_{k,h}^t\left(\mathbf{g}_{k,h}^t\right)^T\succ\mathbf{0}$. Since $\mathbf{g}_{k,i}=\frac{(\mathbf{p}_k-\mathbf{r}_i)}{\|\mathbf{p}_k-\mathbf{r}_i\|_2^2}$, the objective (48) can be cast as

$$\begin{aligned}\phi^{\mathrm{RSS}}(\mathbf{r}_i)&\triangleq\sum_{k=1}^{K}\left(\alpha_{k,i}^t-\frac{(\mathbf{p}_k-\mathbf{r}_i)^T\mathbf{A}_{k,i}^t(\mathbf{p}_k-\mathbf{r}_i)}{\|\mathbf{p}_k-\mathbf{r}_i\|_2^4+(\mathbf{p}_k-\mathbf{r}_i)^T\mathbf{B}_{k,i}^t(\mathbf{p}_k-\mathbf{r}_i)}\right)\\&=\sum_{k=1}^{K}\left(\alpha_{k,i}^t-\psi_k^{\mathrm{RSS}}(\mathbf{r}_i,z_k)\right)\end{aligned} \tag{49}$$

with $z_k=\|\mathbf{p}_k\ d-\mathbf{r}_i\|_2^4+(\mathbf{p}_k\ -\mathbf{r}_i)^T\ \mathbf{B}_{k,i}^t\ (\mathbf{p}_k\ -\mathbf{r}_i)$ and $\psi_k^{\mathrm{RSS}}(\mathbf{r}_i,z)=\frac{(\mathbf{p}_k-\mathbf{r}_i)^T\mathbf{A}_{k,i}^t(\mathbf{p}_k-\mathbf{r}_i)}{z}$. Hence, following lines of reasoning similar to those leading to (38), it can be shown that

$$\left(\mathbf{a}_{k,i}^t\right)^T\mathbf{r}_i-b_{k,i}^tz_k+c_{k,i}^t \tag{50}$$

is a tight lower bound to $\psi_k^{\mathrm{RSS}}(\mathbf{r}_i,z_k)$, where

$$\begin{aligned}\mathbf{a}_{k,i}^t&=\frac{-2\mathbf{A}_{k,i}^t(\mathbf{p}_k-\mathbf{r}_i^t)}{\|\mathbf{p}_k-\mathbf{r}_i^t\|_2^4+(\mathbf{p}_k-\mathbf{r}_i^t)^T\mathbf{B}_{k,i}^t(\mathbf{p}_k-\mathbf{r}_i^t)},\\b_{k,i}^t&=\frac{(\mathbf{p}_k-\mathbf{r}_i^t)^T\mathbf{A}_{k,i}^t(\mathbf{p}_k-\mathbf{r}_i^t)}{\left(\|\mathbf{p}_k-\mathbf{r}_i^t\|_2^4+(\mathbf{p}_k-\mathbf{r}_i^t)^T\mathbf{B}_{k,i}^t(\mathbf{p}_k-\mathbf{r}_i^t)\right)^2},\\c_{k,i}^t&=\psi\left(\mathbf{r}_i^t,z_k^t\right)-\left(\mathbf{a}_{k,i}^t\right)^T\mathbf{r}_i^t+b_{k,i}^tz_k^t.\end{aligned}$$

As consequence, after replacing $z_k=\|\mathbf{p}_k-\mathbf{r}_i\|_2^4+(\mathbf{p}_k-\mathbf{r}_i)^T\mathbf{B}_{k,i}^t(\mathbf{p}_k-\mathbf{r}_i)$ in (50), a majorizing function for $\phi^{\mathrm{RSS}}(\mathbf{r}_i)$ at $\mathbf{r}_i=\mathbf{r}_i^t$ is given by

$$\begin{aligned}\phi^{\mathrm{RSS}}(\mathbf{r}_i)\leq\sum_{k=1}^{K}\Big(&b_{k,i}^t\|\mathbf{p}_k-\mathbf{r}_i\|_2^4+\mathbf{r}_i^T\mathbf{F}_{k,i}^t\mathbf{r}_i\\&-\left(\mathbf{w}_{k,i}^t\right)^T\mathbf{r}_i+\beta_{k,i}^t\Big)\end{aligned} \tag{51}$$

where $\beta_{k,i}^t=\alpha_{k,i}^t-s_{k,i}^t$. Therefore, at the $(t+1)$th iteration, the ith sensor location is updated as the optimal solution to the following surrogate problem

$$\begin{aligned}\underset{\mathbf{r}_i\in\mathcal{R}_i}{\text{minimize}}\ \sum_{k=1}^{K}\Big(&b_{k,i}^t\|\mathbf{p}_k-\mathbf{r}_i\|_2^4+\mathbf{r}_i^T\mathbf{F}_{k,i}^t\mathbf{r}_i\\&-\left(\mathbf{w}_{k,i}^t\right)^T\mathbf{r}_i+\beta_{k,i}^t\Big)\end{aligned} \tag{52}$$

which can be further simplified as

$$\begin{aligned}\underset{\mathbf{r}_i\in\mathcal{R}_i}{\text{minimize}}\ &\sum_{k=1}^{K}\left(b_{k,i}^t\|\mathbf{p}_k-\mathbf{r}_i\|_2^4\right)+\mathbf{r}_i^T\mathbf{F}_i^t\mathbf{r}_i\\&-\left(\mathbf{w}_i^t\right)^T\mathbf{r}_i+\beta_i^t\end{aligned} \tag{53}$$

with $\mathbf{F}_i^t=\sum_{k=1}^{K}\mathbf{F}_{k,i}^t$, $\mathbf{w}_i^t=\sum_{k=1}^{K}\mathbf{w}_{k,i}^t$ and $\beta_i^t=\sum_{k=1}^{K}\beta_{k,i}^t$. Now, to efficiently solve the convex optimization Problem (53), let us introduce K auxiliary variables $\gamma_1,\ldots,\gamma_K$ so as to cast (53) as

$$\begin{aligned}\underset{\mathbf{r}_i\in\mathcal{R}_i,\{\gamma_k\}}{\text{minimize}}\ &\sum_{k=1}^{K}\gamma_k^2+\mathbf{r}_i^T\mathbf{F}_i^t\mathbf{r}_i-\left(\mathbf{w}_i^t\right)^T\mathbf{r}_i+\beta_i^t\\\text{subject to}\ &\sqrt{b_{k,i}^t}\|\mathbf{p}_k-\mathbf{r}_i\|_2^2\leq\gamma_k,\ k=1,\ldots,K.\end{aligned} \tag{54}$$

Provided that $\mathcal{R}_i$ is modeled by means of quadratic and linear inequalities, (54) can be framed as an SOCP and hence readily solved using convex programming solver like CVX [58].

Let us now focus on Problem $\mathcal{P}_3^{RSS}$. Leveraging the functional form of Problem $\mathcal{P}_3^{RSS}$ objective function, the counterpart of Problem (52) can be immediately obtained as follows

$$\begin{aligned}\underset{\mathbf{r}_i\in\mathcal{R}_i}{\text{minimize}}\ &\max_k\Big\{b_{k,i}^t\|\mathbf{p}_k-\mathbf{r}_i\|_2^4+\mathbf{r}_i^T\mathbf{F}_{k,i}^t\mathbf{r}_i\\&-\left(\mathbf{w}_{k,i}^t\right)^T\mathbf{r}_i+\beta_{k,i}^t\Big\}.\end{aligned} \tag{55}$$

Thus, resorting to the epigraph form of (55), the optimization problem to solve for updating the ith sensor position at the tth iteration is

$$\begin{aligned}\underset{\mathbf{r}_i\in\mathcal{R}_i,\theta,\{\gamma_k\}}{\text{minimize}}\ &\theta\\\text{subject to}\ &\sqrt{b_{k,i}^t}\|\mathbf{p}_k-\mathbf{r}_i\|_2^2\leq\gamma_k,\forall k=1,\ldots,K\\&\gamma_k^2+\mathbf{r}_i^T\mathbf{F}_{k,i}^t\mathbf{r}_i-\left(\mathbf{w}_{k,i}^t\right)^T\mathbf{r}_i+\beta_{k,i}^t\leq\theta,\\&k=1,\ldots,K\end{aligned} \tag{56}$$

Since $\mathbf{F}_{k,i}^t\succeq0$, (55) and (56) are convex optimization problems that can be solved using any convex programming solver, in particular, when the constraints allow its SOCP reformulation.

2) Solving Problem $\mathcal{P}_2^{RSS}$ and $\mathcal{P}_4^{RSS}$: In this subsection, the steps to handle $\mathcal{P}_2^{RSS}$ and $\mathcal{P}_4^{RSS}$ are discussed. Following the procedure described to solve $\mathcal{P}_2^{TOA}$ (in Section III-B2), the counterpart of (47) can be written as follows

$$\underset{\mathbf{r}_i\in\mathcal{R}_i}{\text{minimize}}\ \sum_{k=1}^{K}\left(\alpha_{k,i}^t-\frac{\mathbf{g}_{k,i}^T\mathbf{A}_{k,i}^t\mathbf{g}_{k,i}}{1+\mathbf{g}_{k,i}^T\mathbf{B}_{k,i}^t\mathbf{g}_{k,i}}\right) \tag{57}$$

where $\alpha_{k,i}^t\triangleq\det\left(\left(\widetilde{\mathbf{A}}_{k,i}^t\right)^{-1}\right)$, $\mathbf{A}_{k,i}^t\triangleq\sigma_i^{-2}\alpha_{k,i}^t\left(\widetilde{\mathbf{A}}_{k,i}^t\right)^{-1}$, and $\mathbf{B}_{k,i}^t=\sigma_i^{-2}\left(\widetilde{\mathbf{A}}_{k,i}^t\right)^{-1}$.

The form of Problem (57) is similar to (48) in Section III-C1. This implies that optimal solutions to Problem $\mathcal{P}_2^{RSS}$ can be obtained via tools and tricks similar to those explained in Section III-C1. Analogous considerations hold true with reference to $\mathcal{P}_4^{RSS}$ and $\mathcal{P}_4^{TOA}$, paving the way for the synthesis of optimal

sensing geometry according to the design strategy formalized in $\mathcal{P}_4^{RSS}$.

Remark 1: Even though, the CRB for both TOA and RSS looks similar, there are considerable differences between the $\mathbf{H}$ matrix in TOA $\left(\mathbf{h}_{k,i} = \frac{(\mathbf{p}_k - \mathbf{r}_i)}{\|\mathbf{p}_k - \mathbf{r}_i\|_2}\right)$ and $\mathbf{G}$ matrix in RSS $\left(\mathbf{g}_{k,i} = \frac{(\mathbf{p}_k - \mathbf{r}_i)}{\|\mathbf{p}_k - \mathbf{r}_i\|_2^2}\right)$ which make the design problem of optimal sensor placements for RSS-based localization more challenging and worthy of a separate consideration. Indeed, there is an additional $b_{k,i}^t \|\mathbf{p}_k - \mathbf{r}_i\|_2^4$ term in the surrogate function constructed for the concentrated objective function of the ith sensor for the RSS case (see (52)) that has to be carefully dealt with. This implies different mathematical tricks to manage the resulting surrogate function employed and, as a consequence, different optimizations techniques.

The pseudo code to solve Problems $\mathcal{P}_1^{TOA}$–$\mathcal{P}_4^{TOA}$ and $\mathcal{P}_1^{RSS}$–$\mathcal{P}_4^{RSS}$ is given in Algorithm 1.

D. Computational Complexity and Convergence of the Proposed Method

The computational complexity of the proposed algorithm depends on two main factors: the evaluation of the surrogate problem parameters and the computation of the sensor locations update at each iteration. The parameters to be determined are $\mathbf{A}_{k,i}^t$, $\mathbf{D}_{k,i}^t$, $\mathbf{a}_{k,i}^t$, $b_{k,i}^t$ and $c_{k,i}^t$ (for all k and i), and each of them require a complexity of $\mathcal{O}(n^2)$, implying a total burden (per-iteration) of $\mathcal{O}(Kmn^2)$. Moreover, focusing on the most practical situation of quadratic constraints, the update of the sensor locations involves the solution of a SOCP problem[3] which, in turn, can be accomplished with $\mathcal{O}(n^{3.5}\log\eta)$ operations [60], where η is a prescribed accuracy. In summary, the per-iteration complexity is $\mathcal{O}(Kmn^2) + \mathcal{O}(n^{3.5}\log\eta)$.

As to the convergence features of the proposed sensor allocations strategies, leveraging [49], [50], the following proposition holds true.

Proposition 2: Let $\mathcal{P}$ denote one of the design problems $\mathcal{P}_i^{TOA}, \mathcal{P}_i^{RSS}$, $i \in \{1,\ldots,4\}$, $f(\mathbf{r}_1,\ldots,\mathbf{r}_m)$ the associated objective function, and $g_i(\mathbf{r}_i; \mathbf{r}_1^{t+1},\ldots,\mathbf{r}_{i-1}^{t+1}, \mathbf{r}_i^t,\ldots,\mathbf{r}_m^t)$, $i = 1,\ldots,m$, the surrogate function associated with the ith block at the $(t+1)$-iteration, where $\mathbf{r}^t$ refers to the optimal sensor displacement up to the t-iteration. Letting f^t the sequence of objective values attained by $\mathbf{r}^t$, provided that $\widetilde{\mathbf{A}}_{k,i}^t$, $i = 1,\ldots,m$, $k = 1,\ldots,K$, and $t \geq 0$, is full-rank, then

- f^t is a monotonically decreasing function, converging to a finite value;
- any limit point $\mathbf{r}^\star$ of $\mathbf{r}^t$ is a stationary point to $\mathcal{P}$, if the matrices $\widetilde{\mathbf{A}}_{k,i}^{t^\star}$, $i = 1,\ldots,m$, $k = 1,\ldots,K$, evaluated at the limit point $\mathbf{r}^\star$ are full-rank.

Proof: See Appendix A of the supplemental material for proof of the proposition. ■

Remark 3: If the feasible deployment region associated with the ith node is non-convex, its location update can be handled exploiting a tight inner approximation of its feasible set [50] along with the derived objective approximation. For instance, if some of functions involved in the inequality constraints are concave, then they can be linearized, at each loop, using their first order Taylor approximation. Hence, provided that the remaining constraints are convex, the problem resulting at each step is convex and solvable effectively via CVX, for constraint sets of practical interest. Otherwise stated, the proposed approach can effectively deal with these broad design situations resorting to the framework in [50].

[3]It is also worth mentioning that the update demanded by the design based on a average performance can be achieved with a reduced complexity resorting to the KKT conditions.

Algorithm 1: Pseudo code to solve Problems $\mathcal{P}_1^{TOA}$–$\mathcal{P}_4^{TOA}$ and $\mathcal{P}_1^{RSS}$–$\mathcal{P}_4^{RSS}$.

Input: m, n, $\mathbf{R}_{\text{TOA}}$ or $\mathbf{R}_{\text{RSS}}$, K, $\mathbf{p}_1,\ldots,\mathbf{p}_K$, $\epsilon = 10^{-4}$
Initialize $t = 0$, $\mathbf{r}_i^t \in \mathcal{R}_i$ for $i = 1,\ldots,m$ and compute $\mathbf{H}_k^t$ for $k = 1,\ldots,K$.
Repeat:
  for $i = 1,\ldots,m$
    Solve $\mathcal{P}_h^{TOA}$ or $\mathcal{P}_h^{RSS}$, $h = 1, 2, 3,$ and 4:
      if $h = 1$ or $h = 3$
        • Compute $\widetilde{\mathbf{A}}_{k,i}^t$, $\alpha_{k,i}^t$ and $\mathbf{A}_{k,i}^t$ as defined in Section III-B1 for $\mathcal{P}_h^{TOA}$ and Section III-C1 for $\mathcal{P}_h^{RSS}$.
      elseif $h = 2$ or $h = 4$
        • Compute $\widetilde{\mathbf{A}}_{k,i}^t$, $\alpha_{k,i}^t$ and $\mathbf{A}_{k,i}^t$ as defined in Section III-B2 for $\mathcal{P}_h^{TOA}$ and Section III-C2 for $\mathcal{P}_h^{RSS}$.
      end
        • Compute $\mathbf{B}_{k,i}^t$, $\mathbf{D}_{k,i}^t$, $\mathbf{a}_{k,i}^t$, $b_{k,i}^t$, $c_{k,i}^t$, and $s_{k,i}^t$
        • Compute $\mathbf{F}_{k,i}^t$, $\mathbf{w}_{k,i}^t$ and $\beta_{k,i}^t$ using the above parameters.
      if $h = 3$ or $h = 4$
        • $\mathbf{r}_i^{t+1}$ is the solution to the convex problems (44) for $\mathcal{P}_h^{TOA}$ and (56) for $\mathcal{P}_h^{RSS}$.
      elseif $h = 1$ or $h = 2$
        • Compute $\mathbf{F}_i^t = \sum_{k=1}^K \mathbf{F}_{k,i}^t$, $\mathbf{w}_i^t = \sum_{k=1}^K \mathbf{w}_{k,i}^t$ and $\beta_i^t = \sum_{k=1}^K \beta_{k,i}^t$.
        • $\mathbf{r}_i^{t+1}$ is the solution to the convex problems (42) for $\mathcal{P}_h^{TOA}$ and (54) for $\mathcal{P}_h^{RSS}$.
      end
  end
  Compute $\mathbf{H}_k^{t+1}$ for $k = 1,\ldots,K$.
  $t = t + 1$
until convergence
Output: $\{\mathbf{r}_i^*\}$, $\mathbf{r}_i^*$ denote the value of $\mathbf{r}_i$ at convergence.
The convergence criterion is usually $|f(\{\mathbf{r}_i^{t+1}\}) - f(\{\mathbf{r}_i^t\})| < \epsilon$ where $f(\cdot)$ denotes the applicable cost functions in (14)–(17).

IV. Numerical Results

In this section, some interesting case studies are illustrated to assess the performance of the proposed sensor placements strategies under different deployment constraints. In particular, in Subsection IV-A, the design of 2D sensing networks is addressed, whereas in Section IV-B, 3D deployments are considered; furthermore, some results pertaining the performance of the source position maximum likelihood estimator (MLE)

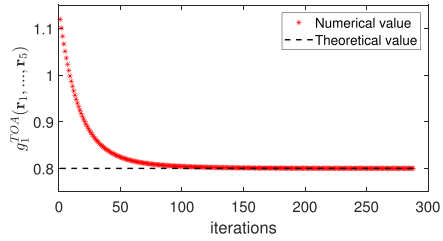

Fig. 2. Objective of Problem $\mathcal{P}_1^{TOA}$ versus iteration index.

relying on noisy measurements gathered by sensors deployed according to different placement strategies are provided in Section IV-C.

Before proceeding further, let us assess the convergence properties of the devised block MM algorithms. To this end, considering $\mathcal{P}_1^{TOA}$ for illustrative purposes, g_1^{TOA} in (11) versus the iteration index is plotted in Fig. 2. Therein, it is assumed $m = 5$, $n = 2$ (2D case), $K = 1$ (only one grid point) located at $(0, 0)$ and $\mathbf{R}_{\text{TOA}} = \mathbf{I}_m$. Besides, in this toy-example, no constraints are enforced[4] and the initial configuration is obtained using uniform placement of sensors on a unit circle with target at its center.

Inspection of the figure shows that the objective value monotonically decreases along the iterations and eventually achieves the theoretical optimal value as computed in [43]. In fact, in such conditions, a placement is optimal if and only if the corresponding matrix $\mathbf{H}$ satisfies [43]

$$\mathbf{H}^T\mathbf{H} = \frac{m}{n}\mathbf{I}_n. \tag{58}$$

In conclusion, Fig. 2 clearly highlights the expected monotonic convergence of the proposed method, also providing an evidence of its effectiveness from an optimization point of view.

A. Sensor Placements in 2D Scenarios

In this subsection, simulation results for the 2D case are illustrated, assuming the source inside a circle of radius r centered at origin. Besides, different sensor deployment regions are considered. Note that, to provide a full picture about the different design methodologies, without overcrowding this section with simulation plots, a few design objectives in each case study are selected and their results are included.

1) Case I: Sensors in Disjoint Angular Sectors: The deployment regions for this case study are represented by the grey striped areas (delimited by blue contours) in Fig. 3, which depict $\mathcal{R}_i$, $i = 1, \ldots, m = 4$. Therein, the outermost circle has a radius of $2r$, whereas the circle tangent to the different regions has a radius $r + \epsilon$, with $\epsilon > 0$. Finally the angular size of each region is $2\pi/m$. As to the parameters[5] settings, $r = 1.5$ Km, $\epsilon = 0.5$, $m = 4$, $K = 100$, $\mathbf{R}_{\text{TOA}} = \text{diag}(0.2500, 0.5625, 1.0000, 2.2500)$, and $\mathbf{R}_{\text{RSS}} = \text{diag}(2.8098, 2.0682, 0.5831, 1.5553)$ are considered.[6,7] Fig. 3(a), (b), and (c) show the optimized placement of $m = 4$ sensors resulting from the optimal solution to $\mathcal{P}_2^{TOA}$, $\mathcal{P}_4^{TOA}$ and $\mathcal{P}_3^{RSS}$, respectively. As expected, all the sensors (displayed by red stars) lie in their respective feasible regions. Besides, different placements arise from diverse measurement models, i.e., TOA/RSS, and/or design metrics. Notably, in all the situations the distance from the origin is not constant, as per the conventional design techniques considered so far in the open literature [5], [43], [61].

TABLE II
COMPARISON OF THE DESIGN OBJECTIVES OBTAINED USING DIFFERENT PLACEMENTS FOR THE 2-D CONFIGURATIONS ANALYZED IN SECTION IV-A1

Sensor Placements	Case I: $\mathbf{R}_{\text{TOA}}$= diag $(0.2500, 0.5625, 1.0000, 2.2500)$ $\mathbf{R}_{\text{RSS}}$=diag $(2.8098, 2.0682, 0.5831, 1.5553)$		
	$g^*_{2,\textbf{TOA}}$	$h^*_{2,\textbf{TOA}}$	$h^*_{1,\textbf{RSS}}$
Random	0.1541	0.2839	18.6298
Uniform	0.0974	0.1459	15.6452
UTMOST[43]	0.0965	0.1732	21.1997
$\mathcal{P}_2^{\text{TOA}}$	**0.0839**	0.1033	37.7327
$\mathcal{P}_4^{\text{TOA}}$	0.0902	**0.1020**	22.5143
$\mathcal{P}_3^{\text{RSS}}$	0.1013	0.1680	**9.6877**

To shed light on the effectiveness of the devised placement strategies, a comparison with some counterparts is now addressed. In this respect, random and uniform placements of the sensors on a circle of radius $r + \epsilon$ are considered; moreover, under the same sensor deployment requirement, the sensor deployments based on the strategy developed in [43], denoted in the following as UTMOST, is also contemplated. In Table II the values of the performance metrics of $\mathcal{P}_2^{TOA}$, $\mathcal{P}_4^{TOA}$, and $\mathcal{P}_3^{RSS}$ are reported for the different sensor configurations. Inspection of the table clearly reveals interesting gains (for each figure of merit) of the tailored layout over the considered counterparts.

2) Case II: Sensor Deployment Regions Modelled as Ellipses: In this situation, each sensor is located in a specific ellipse, where each ellipse is inscribed in a different deployment region as induced by Case I. Specifically, the center of the ith ellipse is at $(\rho\cos(\phi_i), \rho\sin(\phi_i))$, $\rho = 2r$, $\phi_i = (2i - 1)\pi/m$, with the minor axis tangent to the circle of radius ρ. Besides, major and minor axes have a length of $2r/\sqrt{1.5}$ and r, respectively. In this case study, the placements corresponding to $\mathcal{P}_1^{TOA}$, $\mathcal{P}_3^{TOA}$, and $\mathcal{P}_2^{RSS}$ are examined, assuming as simulation parameters $r = 1.5$ Km, $K = 100$, $\mathbf{R}_{\text{TOA}} = \text{diag}(0.1600, 0.6400, 1, 1.4400, 1.9600)$, and $\mathbf{R}_{\text{RSS}} = \text{diag}(0.1788, 0.9275, 0.1101, 1.5723, 0.5604)$. Fig. 4(a), (b), and (c) show the optimized placement of $m = 5$ sensors resulting from the solution to $\mathcal{P}_1^{TOA}$, $\mathcal{P}_3^{TOA}$ and $\mathcal{P}_2^{RSS}$, respectively. Furthermore, Table III reports the objective values (of interest in this subsection) achieved by different sensor configurations (e.g., those based on the heuristic placements defined in Section IV-A1 along with those herein considered). As expected, in

[4]Note that, for $K = 1$ the objective and its restrictions are well defined, but for a zero-measure sensor locations set.

[5]Hereafter, it is assumed that the K points comprising the grid of the assumed source locations are independently drawn from a uniform distribution over the surveillance area $\mathcal{A}$.

[6]Henceforth, the values in the matrices $\mathbf{R}_{\text{TOA}}$ and $\mathbf{R}_{\text{RSS}}$ are in square meters and decibel, respectively.

[7]The path loss component α for the RSS measurement model is set to one in the subsequent experiments.

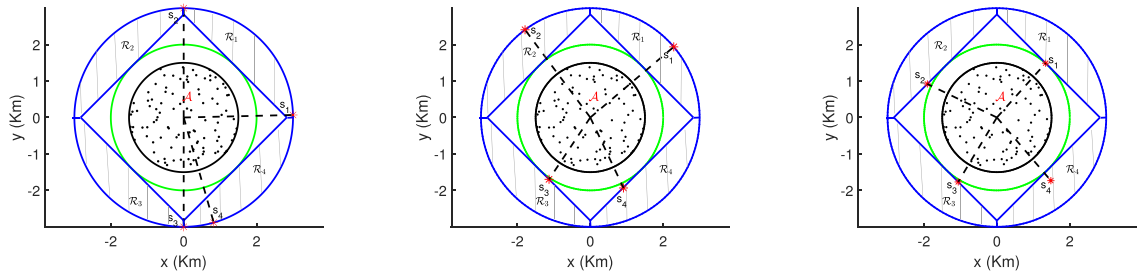

Fig. 3. Optimized sensor positions obtained by solving (a) $\mathcal{P}_2^{\text{TOA}}$, (b) $\mathcal{P}_4^{\text{TOA}}$ and (c) $\mathcal{P}_3^{\text{RSS}}$ with constraint that the ith sensor lies inside the regions $\mathcal{R}_i$. '$\cdot$' markers are the grid points in the source region and red stars are the sensor positions obtained via the developed algorithms.

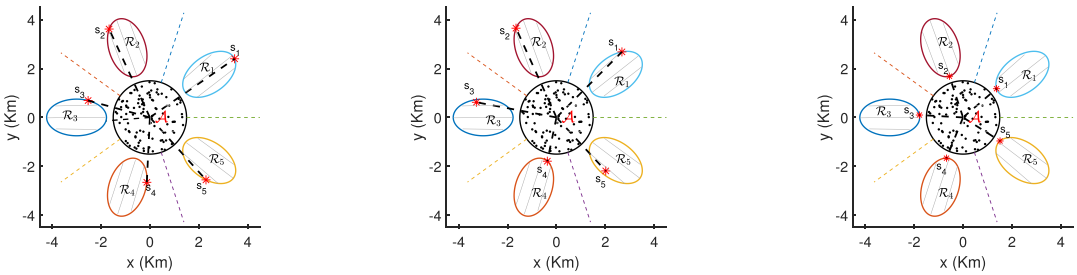

Fig. 4. Optimized sensor positions obtained by solving (a) $\mathcal{P}_1^{TOA}$, (b) $\mathcal{P}_3^{TOA}$ and (c) $\mathcal{P}_2^{RSS}$ with constraint that the ith sensor lies inside the ith ellipse ($\mathcal{R}_i$). '$\cdot$' markers are the grid points in the source region and red stars are the sensor positions.

TABLE III
COMPARISON OF THE DESIGN OBJECTIVES OBTAINED USING DIFFERENT PLACEMENTS FOR THE 2-D CONFIGURATIONS ANALYZED IN SUBSECTION IV-A2

Sensor Placements	Case II: $\mathbf{R}_{\text{TOA}}=$ diag $(0.1600, 0.6400, 1, 1.4400, 1.9600)$ $\mathbf{R}_{\text{RSS}} =$ diag $(0.1788, 0.9275, 0.1101, 1.5723, 0.5604)$		
	$g^*_{1,\textbf{TOA}}$	$h^*_{1,\textbf{TOA}}$	$g^*_{2,\textbf{RSS}}$
Random	1.9688	3.8236	2.4105
Uniform	0.5576	0.7878	0.2148
UTMOST	0.5630	1.0532	1.1075
$\mathcal{P}_1^{TOA}$	0.4933	0.5603	1.8631
$\mathcal{P}_3^{TOA}$	0.5105	0.5409	1.6514
$\mathcal{P}_2^{RSS}$	0.6287	1.0288	0.1277

TABLE IV
COMPARISON OF THE DESIGN OBJECTIVES OBTAINED USING DIFFERENT PLACEMENTS FOR THE 2-D CONFIGURATIONS ANALYZED IN SECTION IV-A3

Sensor Placements	Case III: $\mathbf{R}_{\text{TOA}}=$ diag $(1.0000, 1.1000, 0.9000, 1.3000)$ $\mathbf{R}_{\text{RSS}} =$ diag $(0.2297, 0.8270, 0.8319, 0.4978)$		
	$g^*_{1,\textbf{TOA}}$	$g^*_{1,\textbf{RSS}}$	$h^*_{2,\textbf{RSS}}$
Random	1.6278	5.9409	7.8632
Uniform	1.1083	2.4838	1.8255
UTMOST	1.1967	2.7679	3.6567
$\mathcal{P}_1^{TOA}$	1.0887	4.8615	5.3892
$\mathcal{P}_1^{RSS}$	1.1837	1.8721	3.3722
$\mathcal{P}_4^{RSS}$	1.1439	2.6175	1.7538

each column the lowest objective value is achieved by the sensor configurations driven by the bespoke design. Besides, the differences among the reported objective values corroborate the presence of distinct topological behavior in Fig. 4.

3) Case III: Sensors in an Annular Region: In this case the sensors are constrained to lie inside the annular region $\mathcal{R} = \mathcal{R}_1 =, \ldots, = \mathcal{R}_m = \{\mathbf{r} : r + \epsilon \leq \|\mathbf{r}\|^2 \leq 2r\}$, see the grey-striped area in Fig. 5. This feasible set is non-convex due to the requirement $\|\mathbf{r}\|^2 \geq r + \epsilon$. However, a viable means to handle such a design is to resort to the approach discussed in Remark 3. The parameters settings chosen in this simulation are $r = 1.5$ Km, $\epsilon = 0.5$ Km, $K = 100$, $\mathbf{R}_{\text{TOA}} = \text{diag}(1.0000, 1.1000, 0.9000, 1.3000)$, and $\mathbf{R}_{\text{RSS}} = \text{diag}(0.2297, 0.8270, 0.8319, 0.4978)$. Fig. 5(a), (b), and (c) show the optimized placement of $m = 4$ sensors obtained by solving problems $\mathcal{P}_1^{TOA}$, $\mathcal{P}_1^{RSS}$ and $\mathcal{P}_4^{RSS}$, respectively, under this specific restriction for the sensor locations. Finally, the results in Table IV confirm the effectiveness of the proposed design methods.

B. Sensor Placements in 3D Scenarios

In this subsection, sensor deployments optimization in a 3D space is addressed, assuming that the source lies inside the volume specified by the sphere ($\mathcal{S}_1$) of radius r centered at origin of the reference system. The following deployment regions are considered.

1) Case I: Sensors Inside Ellipsoids: In this scenario, the deployment regions are given by m equally sized ellipsoids, each with an axis parallel to the y-axis. Their centers are uniformly spaced into the x-z plane at a distance $2r$ from

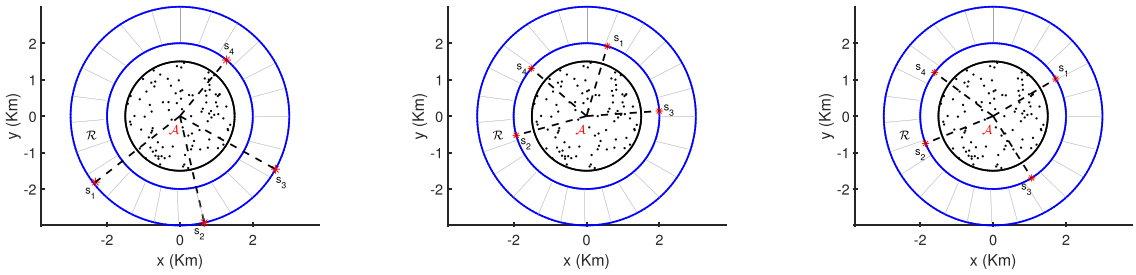

Fig. 5. Optimized sensor positions obtained by solving (a) $\mathcal{P}_1^{TOA}$, (b) $\mathcal{P}_1^{RSS}$ and (c) $\mathcal{P}_4^{RSS}$ with constraint that the sensors lie in the annular region $\mathcal{R}$. '$\cdot$' markers are the grid points in the source region and red stars are the sensor positions.

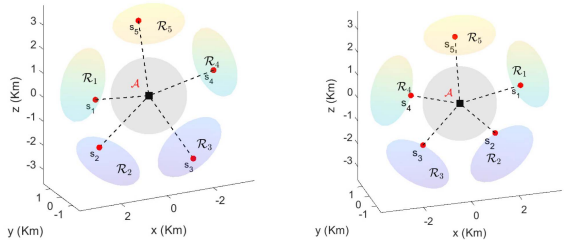

Fig. 6. Optimized sensor positions obtained by solving (a) $\mathcal{P}_1^{TOA}$ and (b) $\mathcal{P}_1^{RSS}$ with constraint that the ith sensor lies inside $\mathcal{R}_i$. Red circles are the sensor positions obtained via our developed algorithm.

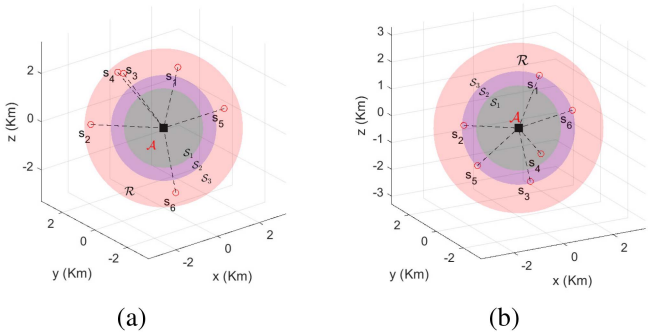

Fig. 7. Optimized sensor positions obtained by solving (a) $\mathcal{P}_3^{TOA}$ and (b) $\mathcal{P}_3^{RSS}$ with constraint that the sensors lie in an annular region $\mathcal{R}$. Red circles are the sensor positions obtained via our algorithm.

TABLE V
COMPARISON OF THE DESIGN OBJECTIVES OBTAINED USING DIFFERENT PLACEMENTS FOR THE 3-D CONFIGURATIONS ANALYZED IN SUBSECTION IV-B1

Sensor Placements	Case I: $\mathbf{R}_{\text{TOA}}$= diag $(0.1600, 0.3600, 0.6400, 1.0000, 1.4400)$ $\mathbf{R}_{\text{RSS}}$ = diag $(0.8783, 0.6477, 1.0495, 1.3230, 0.5173)$	
	$g^*_{1,\textbf{TOA}}$	$g^*_{1,\textbf{RSS}}$
Random	3.5344	78.6578
UTMOST	1.5629	60.8343
$\mathcal{P}_1^{TOA}$	1.3649	21.9223
$\mathcal{P}_1^{\text{RSS}}$	2.3522	17.0625

TABLE VI
COMPARISON OF THE DESIGN OBJECTIVES OBTAINED USING DIFFERENT PLACEMENTS FOR THE 3-D CONFIGURATIONS ANALYZED IN SUBSECTION IV-B2

Sensor Placements	Case II: $\mathbf{R}_{\text{TOA}}$= diag $(0.0625, 0.2500, 0.5625, 1.0000, 1.5625, 2.2500)$ $\mathbf{R}_{\text{RSS}}$ = $(0.9319, 0.3579, 0.2021, 0.8763, 0.8079, 1.6033)$	
	$h^*_{1,\textbf{TOA}}$	$h^*_{1,\textbf{RSS}}$
Random	5.3724	21.7676
UTMOST	1.8579	16.6451
$\mathcal{P}_3^{TOA}$	1.2997	10.3067
$\mathcal{P}_3^{RSS}$	1.8081	7.0246

the origin with the major axis tangent to the circle of radius $2r$. Specifically, the three ellipsoids are congruent with axes of sizes $2r$, and r into the x-z plane, and $\sqrt{2}r$ along the y axis. Hence, the ith sensor is constrained to lie within the ith ellipsoid. Assuming $r = 1.5$ Km, $m = 5$, $K = 150$, $\mathbf{R}_{\text{TOA}} = \text{diag}(0.1600, 0.3600, 0.6400, 1.0000, 1.4400)$, and $\mathbf{R}_{\text{RSS}} = \text{diag}(0.8783, 0.6477, 1.0495, 1.3230, 0.5173)$ in Fig. 6(a) and (b), the optimized sensor placements obtained by solving problems $\mathcal{P}_1^{TOA}$ and $\mathcal{P}_1^{RSS}$ under this specific constraint are displayed. The analysis clearly unveils the influence of the measurement model on the placement. In Table V, the values of the performance metrics associated with $\mathcal{P}_1^{TOA}$ and $\mathcal{P}_1^{RSS}$ are reported versus the sensor configurations. Again, the lowest value of each figure of merit is attained by the configuration driven by its minimization via the novel placement tool.

2) Case II: Sensors in an Annular Region: In this scenario, the sensors are constrained to lie in an annular region corresponding to the points of the sphere $\mathcal{S}_3$ which do not belong to $\mathcal{S}_2$. Similar to the 2D case, the constraint set is non-convex because of the requirement $\|\mathbf{r}\|^2 \geq r + \epsilon$. Therefore, resorting to the MM framework, a convex and tight inner bound to the feasible set can be determined by means of the first order Taylor's expansion of $-\|\mathbf{r}_i\|^2$ at the previous location of the ith sensor, i.e., r_i^t, along the optimization process. As to the parameters setting, it is assumed $r = 1.5$ Km, $m = 6$, $K = 150$, $\mathbf{R}_{\text{TOA}} = \text{diag}(0.0625, 0.2500, 0.5625, 1.0000, 1.5625, 2.2500)$ and $\mathbf{R}_{\text{RSS}} = \text{diag}(0.9319, 0.3579, 0.2021, 0.8763, 0.8079, 1.6033)$. Fig. 7(a) and (b) show the optimized sensor placements for $\mathcal{P}_3^{TOA}$ and $\mathcal{P}_3^{RSS}$, respectively. Again the impact of the measurement model is clearly pinpointed. Finally, the objective values in Table VI further assert the strength of the proposed algorithms.

TABLE VII
COMPARISON OF THE MLE PERFORMANCE FOR DIFFERENT PLACEMENT ASSUMING TOA BASED LOCALIZATION

Simulation parameters	Placement	Average MSE (m^2)	Worst-case MSE (m^2)
$m=4, n=2, K=100$ $\mathbf{R}_{\text{TOA}}=$ diag $(0.1741, 0.6764, 0.4879, 0.9966)$	Random	0.270	0.493
	Uniform	0.166	0.223
	UTMOST	0.190	0.280
	Proposed*	0.154	0.175
	Proposed†	0.158	0.174
$m=5, n=2, K=100$ $\mathbf{R}_{\text{TOA}}=$ diag $(0.8896, 0.8215, 1.1401, 0.3907, 1.7578)$	Random	0.291	0.608
	Uniform	0.185	0.254
	UTMOST	0.181	0.220
	Proposed*	0.165	0.200
	Proposed†	0.169	0.174
$m=6, n=2, K=100$ $\mathbf{R}_{\text{TOA}}=$ diag $(0.9794, 0.2972, 0.8295, 0.8084, 1.9083, 0.2651)$	Random	0.196	0.440
	Uniform	0.151	0.193
	UTMOST	0.149	0.163
	Proposed*	0.143	0.149
	Proposed†	0.143	0.147

*Averaged $A-$optimal design
†Worst-case $A-$optimal design

C. MSE Comparison

This subsection is aimed at shedding light on the performance benefits offered by the proposed sensor deployment strategies in terms of localization MSE improvements. To this end the MLE is used to perform source localization[8] with respect to TOA. Besides, a 2D scenario with a circle of radius 0.75 Km centered at $(0, 0)$ as source area is supposed at the design stage. $K = 100$ is used to formalize the sensor placements problems based on the average $A-$optimal and worst-case $A-$optimal design metrics for TOA based localization.

To assess the MLE performance under the different configurations, the MSE values associated with 10 source positions (randomly selected within the surveillance region) are computed. Then, the average and the maximum (worst-case) MSE (of the MLE) are adopted as synthetic benchmarks of quality. For comparison purposes, the localization capabilities of sensor networks resulting from different placement approaches including UTMOST are analyzed too.[9] Notably, the randomly selected source positions, in correspondence of which the MSE values (associated with the MLE) are obtained, differ from the assumed locations (via the grid points) with probability one. In a nutshell, the analysis in this subsection offers insights into the performance of the proposed method in the case of source position mismatches against the selected grid of points supposed at the resource allocation stage.

Table VII reports the average and maximum MSE (of the MLE) for different values of m and interference variances, where at each source location 1000 Monte Carlo trials are performed. Inspection of the table reveals the effectiveness of the proposed resource allocation algorithms with notable performance gains as compared with possible counterparts. In particular, the average $A-$optimal design usually provides the best average MSE in each case study, whereas worst-case $A-$optimal approach offers in general benefits in terms of worst-case MSE. This validates our claim that the method proposed in this paper is indeed capable of endowing robustness to the sensor placements against the actual source location within the surveillance region, even in the presence of possible deviations among the selected grid of points and the effective source position.

[8]The TOA MLE has been implemented by performing first a grid search to obtain an approximated solution of the optimization problem underlying the MLE; then the source position estimate is further refined using the Gauss Newton algorithm.

[9]Note that, the design resulting from the proposed algorithm assumes that the sensors are constrained to lie in an annular region.

V. CONCLUSION

In this paper, a robust method that designs the optimal sensor positions for TOA and RSS based source localization has been developed. The proposed approach does not rely on the actual source location but just considers a quite general surveillance area/volume that contains the actual source, and minimizes average and worst-case CRB-related metrics over the grid points sampling the surveillance area/volume. Besides, unlike most of the state-of-the-art techniques, the design variables are the sensor positions and not only their orientations. The developed framework, based on block-MM technique, has been applied to both $A-$ and $D-$ optimal designs, and is capable of effectively handling non-uniform measurement noise variances and general sensor deployment constraints. Numerical simulations have shown that the new techniques endow robustness to the deployment process and can outperform a current state-of-the art algorithm to design optimized sensor locations. Possible future research avenues could be focused on the extension of the techniques to TDOA and hybrid TOA-RSS-TDOA based localization, as well as to tracking applications where a figure of merit accounting for the accuracy of the target trajectory estimate is considered.

REFERENCES

[1] D. Li, K. D. Wong, Y. Hen Hu, and A. M. Sayeed, "Detection, classification, and tracking of targets," *IEEE Signal Process. Mag.*, vol. 19, no. 2, pp. 17–29, Mar. 2002.
[2] J. Moreau, S. Ambellouis, and Y. Ruichek, "Fisheye-based method for GPS localization improvement in unknown semi-obstructed areas," *Sensors*, vol. 17, no. 1, 2017, Art. no. 119.
[3] H. Godrich, A. P. Petropulu, and H. V. Poor, "Power allocation strategies for target localization in distributed multiple-radar architectures," *IEEE Trans. Signal Process.*, vol. 59, no. 7, pp. 3226–3240, Jul. 2011.
[4] M. Leonardi, A. Mathias, and G. Galati, "Two efficient localization algorithms for multilateration," *Int. J. Microw. Wireless Technol.*, vol. 1, no. 3, pp. 223–229, 2009.
[5] J. Shen, A. F. Molisch, and J. Salmi, "Accurate passive location estimation using TOA measurements," *IEEE Trans. Wireless Commun.*, vol. 11, no. 6, pp. 2182–2192, Jun. 2012.
[6] B. Huang, L. Xie, and Z. Yang, "TDOA-based source localization with distance-dependent noises," *IEEE Trans. Wireless Commun.*, vol. 14, no. 1, pp. 468–480, Jan. 2015.
[7] A. J. Weiss, "On the accuracy of a cellular location system based on RSS measurements," *IEEE Trans. Veh. Technol.*, vol. 52, no. 6, pp. 1508–1518, Nov. 2003.
[8] Y. Zhu, D. Huang, and A. Jiang, "Network localization using angle of arrival," in *Proc. IEEE Int. Conf. Electro/Inf. Technol.*, 2008, pp. 205–210.
[9] K. C. Ho and W. Xu, "An accurate algebraic solution for moving source location using TDOA and FDOA measurements," *IEEE Trans. Signal Process.*, vol. 52, no. 9, pp. 2453–2463, Sep. 2004.
[10] K. Yoo, J. Chun, and C. Ryu, "CRB-based optimal radar placement for target positioning," in *Proc. IEEE Int. Conf. Radar*, 2018, pp. 1–5.

[11] K. Yoo and J. Chun, "Analysis of optimal range sensor placement for tracking a moving target," *IEEE Commun. Lett.*, vol. 24, no. 8, pp. 1700–1704, Aug. 2020.

[12] K. Doğançay and H. Hmam, "Optimal angular sensor separation for AOA localization," *Signal Process.*, vol. 88, no. 5, pp. 1248–1260, 2008.

[13] D. Moreno-Salinas, A. Pascoal, and J. Aranda, "Sensor networks for optimal target localization with bearings-only measurements in constrained three-dimensional scenarios," *Sensors*, vol. 13, no. 8, pp. 10386–10417, 2013.

[14] S. Xu and K. Doğançay, "Optimal sensor deployment for 3D AOA target localization," in *Proc. IEEE Int. Conf. Acoust., Speech, Signal Process.*, 2015, pp. 2544–2548.

[15] S. Xu and K. Doğançay, "Optimal sensor placement for 3-D angle-of-arrival target localization," *IEEE Trans. Aerosp. Electron. Syst.*, vol. 53, no. 3, pp. 1196–1211, Jun. 2017.

[16] X. Fang and J. Li, "Frame theory for optimal sensor augmentation problem of AOA localization," *IEEE Signal Process. Lett.*, vol. 25, no. 9, pp. 1310–1314, Sep. 2018.

[17] Y. Zheng, J. Liu, M. Sheng, S. Han, Y. Shi, and S. Valaee, "Toward practical access point deployment for angle-of-arrival based localization," *IEEE Trans. Commun.*, vol. 69, no. 3, pp. 2002–2014, Mar. 2021.

[18] M. Hamdollahzadeh, R. Amiri, and F. Behnia, "Optimal sensor placement for multi-source AOA localisation with distance-dependent noise model," *IET Radar, Sonar Navigation*, vol. 13, no. 6, pp. 881–891, 2019.

[19] X. Fang, J. Li, S. Zhang, W. Chen, and Z. He, "Optimal AOA sensor-source geometry with deployment region constraints," *IEEE Commun. Lett.*, vol. 26, no. 4, pp. 793–797, Apr. 2022.

[20] K. Dogancay, "Optimal geometries for AOA localization in the Bayesian sense," *Sensors*, vol. 22, no. 24, 2022, Art. no. 9802.

[21] B. Yang and J. Scheuing, "Cramer-Rao bound and optimum sensor array for source localization from time differences of arrival," in *Proc. IEEE Int. Conf. Acoust., Speech, Signal Process.*, 2005, pp. iv-961–iv/964.

[22] J. T. Isaacs, D. J. Klein, and J. P. Hespanha, "Optimal sensor placement for time difference of arrival localization," in *Proc. IEEE 48th Conf. Decis. Control, Jointly 8th Chin. Control Conf.*, 2009, pp. 7878–7884.

[23] D. Moreno-Salinas, A. M. Pascoal, and J. Aranda, "Optimal sensor placement for multiple underwater target localization with acoustic range measurements," *IFAC Proc. Vol.*, vol. 44, no. 1, pp. 12825–12832, 2011.

[24] L. Rui and K. C. Ho, "Elliptic localization: Performance study and optimum receiver placement," *IEEE Trans. Signal Process.*, vol. 62, no. 18, pp. 4673–4688, Sep. 2014.

[25] W. Meng, L. Xie, and W. Xiao, "Optimal TDOA sensor-pair placement with uncertainty in source location," *IEEE Trans. Veh. Technol.*, vol. 65, no. 11, pp. 9260–9271, Nov. 2016.

[26] N. H. Nguyen and K. Doğançay, "Optimal geometry analysis for multistatic TOA localization," *IEEE Trans. Signal Process.*, vol. 64, no. 16, pp. 4180–4193, Aug. 2016.

[27] S. Gezici, S. Bayram, M. N. Kurt, and M. R. Gholami, "Optimal jammer placement in wireless localization systems," *IEEE Trans. Signal Process.*, vol. 64, no. 17, pp. 4534–4549, Sep. 2016.

[28] D. Moreno-Salinas, A. Pascoal, and J. Aranda, "Optimal sensor placement for acoustic underwater target positioning with range-only measurements," *IEEE J. Ocean. Eng.*, vol. 41, no. 3, pp. 620–643, Jul. 2016.

[29] A. Comuniello, A. Moschitta, and A. De Angelis, "Ultrasound TDoA positioning using the best linear unbiased estimator and efficient anchor placement," *IEEE Trans. Instrum. Meas.*, vol. 69, no. 5, pp. 2477–2486, May 2019.

[30] S. Xu, Y. Ou, and X. Wu, "Optimal sensor placement for 3-D time-of-arrival target localization," *IEEE Trans. Signal Process.*, vol. 67, no. 19, pp. 5018–5031, Oct. 2019.

[31] S. Xu, M. Rice, and F. Rice, "Optimal TOA-sensor placement for two target localization simultaneously using shared sensors," *IEEE Commun. Lett.*, vol. 25, no. 8, pp. 2584–2588, Aug. 2021.

[32] M. Sadeghi, F. Behnia, and R. Amiri, "Optimal sensor placement for 2-D range-only target localization in constrained sensor geometry," *IEEE Trans. Signal Process.*, vol. 68, pp. 2316–2327, 2020.

[33] M. Sadeghi, F. Behnia, and R. Amiri, "Optimal geometry analysis for TDOA-based localization under communication constraints," *IEEE Trans. Aerosp. Electron. Syst.*, vol. 57, no. 5, pp. 3096–3106, Oct. 2021.

[34] A. N. Bishop and P. Jensfelt, "An optimality analysis of sensor-target geometries for signal strength based localization," in *Proc. Int. Conf. Intell. Sensors, Sensor Netw., Inf. Process.*, 2009, pp. 127–132.

[35] A. E. C. Redondi and E. Amaldi, "Optimizing the placement of anchor nodes in RSS-based indoor localization systems," in *Proc. 12th Annu. Mediterranean Ad Hoc Netw. Workshop*, 2013, pp. 8–13.

[36] S. Xu, Y. Ou, and W. Zheng, "Optimal sensor-target geometries for 3-D static target localization using received-signal-strength measurements," *IEEE Signal Process. Lett.*, vol. 26, no. 7, pp. 966–970, Jul. 2019.

[37] A. Heydari, M. Aghabozorgi, and M. Biguesh, "Optimal sensor placement for source localization based on RSSD," *Wireless Netw.*, vol. 26, no. 7, pp. 5151–5162, 2020.

[38] H. Hmam, "Optimal sensor velocity configuration for TDOA-FDOA geolocation," *IEEE Trans. Signal Process.*, vol. 65, no. 3, pp. 628–637, Feb. 2017.

[39] W. Wang, P. Bai, Y. Wang, X. Liang, and J. Zhang, "Optimal sensor deployment and velocity configuration with hybrid TDOA and FDOA measurements," *IEEE Access*, vol. 7, pp. 109181–109194, 2019.

[40] S. Xu, "Optimal sensor placement for target localization using hybrid RSS, AOA and TOA measurements," *IEEE Commun. Lett.*, vol. 24, no. 9, pp. 1966–1970, Sep. 2020.

[41] K. Panwar, G. Fatima, and P. Babu, "Optimal sensor placement for hybrid source localization using fused TOA-RSS-AOA measurements," *IEEE Trans. Aerosp. Electron. Syst.*, vol. 59, no. 2, pp. 1643–1657, Apr. 2023, doi: 10.1109/TAES.2022.3202879.

[42] Y. Liang and Y. Jia, "Constrained optimal placements of heterogeneous range/bearing/RSS sensor networks for source localization with distance-dependent noise," *IEEE Geosci. Remote Sens. Lett.*, vol. 13, no. 11, pp. 1611–1615, Nov. 2016.

[43] N. Sahu, L. Wu, P. Babu, B. S. M. R., and B. Ottersten, "Optimal sensor placement for source localization: A unified ADMM approach," *IEEE Trans. Veh. Technol.*, vol. 71, no. 4, pp. 4359–4372, Apr. 2022.

[44] Y.-T. Chan and F. L. Jardine, "Target localization and tracking from Doppler-shift measurements," *IEEE J. Ocean. Eng.*, vol. 15, no. 3, pp. 251–257, Jul. 1990.

[45] I. Shames, A. N. Bishop, M. Smith, and B. D. Anderson, "Doppler shift target localization," *IEEE Trans. Aerosp. Electron. Syst.*, vol. 49, no. 1, pp. 266–276, Jan. 2013.

[46] M. B. Guldogan, D. Lindgren, F. Gustafsson, H. Habberstad, and U. Orguner, "Multi-target tracking with PHD filter using doppler-only measurements," *Digit. Signal Process.*, vol. 27, pp. 1–11, 2014.

[47] N. H. Nguyen and K. Doğançay, "Optimal sensor placement for doppler shift target localization," in *Proc. IEEE Radar Conf.*, 2015, pp. 1677–1682.

[48] Y. Li, G. Qi, and A. Sheng, "Optimal deployment of vehicles with circular formation for bearings-only multi-target localization," *Automatica*, vol. 105, pp. 347–355, 2019.

[49] M. Razaviyayn, M. Hong, and Z.-Q. Luo, "A unified convergence analysis of block successive minimization methods for nonsmooth optimization," *SIAM J. Optim.*, vol. 23, no. 2, pp. 1126–1153, 2013.

[50] A. Aubry, A. De Maio, A. Zappone, M. Razaviyayn, and Z.-Q. Luo, "A new sequential optimization procedure and its applications to resource allocation for wireless systems," *IEEE Trans. Signal Process.*, vol. 66, no. 24, pp. 6518–6533, Dec. 2018.

[51] D. Slepian, "Estimation of signal parameters in the presence of noise," *Trans. IRE Professional Group Inf. Theory*, vol. 3, no. 3, pp. 68–89, 1954.

[52] D. Ucinski, *Optimal Measurement Methods for Distributed Parameter System Identification*. Boca Raton, FL, USA:CRC Press, 2004.

[53] H. C. So, "Source localization: Algorithms and analysis," *Handbook of Position Location: Theory, Practice, and Advances*. Piscataway, NJ, USA: Wiley, 2011, pp. 25–66.

[54] N. Patwari, A. O. Hero, M. Perkins, N. S. Correal, and R. J. O'dea, "Relative location estimation in wireless sensor networks," *IEEE Trans. Signal Process.*, vol. 51, no. 8, pp. 2137–2148, Aug. 2003.

[55] Y. Sun, P. Babu, and D. P. Palomar, "Majorization-minimization algorithms in signal processing, communications, and machine learning," *IEEE Trans. Signal Process.*, vol. 65, no. 3, pp. 794–816, Feb. 2017.

[56] W. H. Press, S. A. Teukolsky, W. T. Vetterling, and B. P. Flannery, *Numerical Recipes: The Art of Scientific Computing*, 3rd ed. Cambridge, U.K.: Cambridge Univ. Press, 2007.

[57] S. Boyd, S. P. Boyd, and L. Vandenberghe, *Convex Optimization*. Cambridge, U.K.: Cambridge Univ. Press, 2004.

[58] M. Grant and S. Boyd, "CVX: Matlab software for disciplined convex programming, version 2.1," Mar. 2014. [Online]. Available: http://cvxr.com/cvx

[59] D. A. Harville, *Matrix Algebra From a Statistician's Perspective*. New York, NY, USA: Taylor & Francis, 1998.

[60] A. Ben-Tal, L. El Ghaoui, and A. Nemirovski, *Robust Optimization*, vol. 28. Princeton, NJ, USA: Princeton Univ. Press, 2009.

[61] X. Fang, W. Yan, F. Zhang, and J. Li, "Optimal sensor placement for range-based dynamic random localization," *IEEE Geosci. Remote Sens. Lett.*, vol. 12, no. 12, pp. 2393–2397, Dec. 2015.